Theses and Dissertations   1. Thesis and Dissertation Collection, all items

2005-12

System study and design of broad-band U-Slot microstrip patch antennas for aperstructures and opportunistic arrays

Tong, Chin Hong Matthew

Monterey California. Naval Postgraduate School

http://hdl.handle.net/10945/1802

NAVAL
POSTGRADUATE
SCHOOL

MONTEREY, CALIFORNIA

THESIS

SYSTEM STUDY AND DESIGN OF BROAD-BAND U-SLOT MICROSTRIP PATCH ANTENNAS FOR APERSTRUCTURES AND OPPORTUNISTIC ARRAYS

by

Tong, Chin Hong Matthew

December 2005

Thesis Advisor: David C. Jenn
Co-Advisor: Donald L. Walters

Approved for public release; distribution is unlimited

THIS PAGE INTENTIONALLY LEFT BLANK

REPORT DOCUMENTATION PAGE			*Form Approved OMB No. 0704-0188*
Public reporting burden for this collection of information is estimated to average 1 hour per response, including the time for reviewing instruction, searching existing data sources, gathering and maintaining the data needed, and completing and reviewing the collection of information. Send comments regarding this burden estimate or any other aspect of this collection of information, including suggestions for reducing this burden, to Washington headquarters Services, Directorate for Information Operations and Reports, 1215 Jefferson Davis Highway, Suite 1204, Arlington, VA 22202-4302, and to the Office of Management and Budget, Paperwork Reduction Project (0704-0188) Washington DC 20503.			
1. AGENCY USE ONLY *(Leave blank)*	**2. REPORT DATE** December 2005	**3. REPORT TYPE AND DATES COVERED** Master's Thesis	
4. TITLE AND SUBTITLE: System Study and Design of Broad-band U-Slot Microstrip Patch Antennas for Aperstructures and Opportunistic Arrays		**5. FUNDING NUMBERS**	
6. AUTHOR(S) Tong, Chin Hong Matthew			
7. PERFORMING ORGANIZATION NAME(S) AND ADDRESS(ES) Naval Postgraduate School Monterey, CA 93943-5000		**8. PERFORMING ORGANIZATION REPORT NUMBER**	
9. SPONSORING /MONITORING AGENCY NAME(S) AND ADDRESS(ES) N/A		**10. SPONSORING/MONITORING AGENCY REPORT NUMBER**	
11. SUPPLEMENTARY NOTES The views expressed in this thesis are those of the author and do not reflect the official policy or position of the Department of Defense or the U.S. Government.			
12a. DISTRIBUTION / AVAILABILITY STATEMENT Approved for public release; distribution is unlimited		**12b. DISTRIBUTION CODE**	
13. ABSTRACT (maximum 200 words)			

An opportunistic array is an integrated ship-wide digital phased-array radar, where antenna elements are placed at available open areas over the entire ship's length. Such an array has the potential to fulfill many of the Navy's missions, including ballistic missile defence (BMD) where the radar mission encompasses exo-atmospheric surveillance, tracking and preliminary discrimination. Advantages of opportunistic arrays include enhanced stealth – since low-profile antennas reduce the ship's RCS; high angular resolution – as the entire ship's length forms the "aperture" and produces a narrow beamwidth; and potentially lower costs – through the use of COTS technology and a flexible digital antenna architecture that reduces the number of distinct radar systems required.

This research first investigated the opportunistic array concept in the context of BMD. A system level tradeoff was performed to size the system and verify that detection ranges greater than 1000 km could be achieved. Next, the research focused on designing a low-profile, broad-band U-slot microstrip patch antenna. Theoretical calculations and parametric studies were performed to develop an antenna element that could operate in the upper VHF/lower UHF frequencies. A set of simple design procedures is proposed to provide approximate rules that result in a good "first-pass" design with prescribed characteristics that require minimal tuning.

14. SUBJECT TERMS Aperstructure, Opportunistic Array, U-Slot, Microstrip Patch Antenna, Ballistic Missile Defence (BMD), Broad-band			**15. NUMBER OF PAGES** 108
			16. PRICE CODE
17. SECURITY CLASSIFICATION OF REPORT Unclassified	**18. SECURITY CLASSIFICATION OF THIS PAGE** Unclassified	**19. SECURITY CLASSIFICATION OF ABSTRACT** Unclassified	**20. LIMITATION OF ABSTRACT** UL

i

THIS PAGE INTENTIONALLY LEFT BLANK

SYSTEM STUDY AND DESIGN OF BROADBAND U-SLOT MICROSTRIP PATCH ANTENNAS FOR APERSTRUCTURES AND OPPORTUNISTIC ARRAYS

Chin Hong Matthew Tong
Captain, Singapore Army
B.S., Cornell University, 1999
M.Eng., Cornell University, 2000

Submitted in partial fulfillment of the
requirements for the degree of

MASTER OF SCIENCE IN COMBAT SYSTEMS TECHNOLOGY

from the

**NAVAL POSTGRADUATE SCHOOL
December 2005**

Author: Chin Hong Matthew Tong

Approved by: David C. Jenn
                   Thesis Advisor

                   Donald L. Walters
                   Co-Advisor

                   James Luscombe
                   Chairman, Department of Physics

iii

THIS PAGE INTENTIONALLY LEFT BLANK

ABSTRACT

An opportunistic array is an integrated ship-wide digital phased-array radar, where antenna elements are placed at available open areas over the entire ship's length. Such an array has the potential to fulfill many of the Navy's missions, including ballistic missile defence (BMD) where the radar mission encompasses exo-atmospheric surveillance, tracking and preliminary discrimination. Advantages of opportunistic arrays include enhanced stealth – since low-profile antennas reduce the ship's RCS; high angular resolution – as the entire ship's length forms the "aperture" and produces a narrow beamwidth; and potentially lower costs – through the use of COTS technology and a flexible digital antenna architecture that reduces the number of distinct radar systems required.

This research first investigated the opportunistic array concept in the context of BMD. A system level tradeoff was performed to size the system and verify that detection ranges greater than 1000 km could be achieved. Next, the research focused on designing a low-profile, broad-band U-slot microstrip patch antenna. Theoretical calculations and parametric studies were performed to develop an antenna element that could operate in the upper VHF/lower UHF frequencies. A set of simple design procedures is proposed to provide approximate rules that result in a good "first-pass" design with prescribed characteristics that require minimal tuning.

THIS PAGE INTENTIONALLY LEFT BLANK

TABLE OF CONTENTS

LIST OF FIGURES

xii

THIS PAGE INTENTIONALLY LEFT BLANK

LIST OF TABLES

THIS PAGE INTENTIONALLY LEFT BLANK

ACKNOWLEDGMENTS

I wish to express my deepest thanks to my wife, Dawn, for her love and support throughout the course of my research and study.

I would like to thank my thesis advisor, Professor David C. Jenn, for his excellent guidance and invaluable support. Many thanks for always being patient with my questions and available to help, even late in the evenings. I am also grateful to my thesis co-advisor, Professor Donald L. Walters, for his valuable advice and discussions.

Special thanks to my coursemates, LTC Yong, Yoke Chuang and Mr Winston Ong, who worked on the same project and were a source of great friendship, encouragement and support.

THIS PAGE INTENTIONALLY LEFT BLANK

I.   INTRODUCTION

> Tomorrow's Navy is about projecting not just offense, but projecting defense hundreds and even thousands of miles away.
>
> - Admiral Vern Clark, U.S. Navy [1]

A.   MOTIVATION

Tomorrow's Navy faces an era characterized by shifting global threats, unrestricted warfare as well as challenging new opportunities. Seizing on these new opportunities, Sea Power 21 articulated a vision for a "combat ready Navy – forward-deployed, rotational and surge capable – large enough, agile enough and lethal enough to deter any threat and defeat any foe in support of the Joint Force" [2]. This thesis examines the concept of aperstructures and opportunistic arrays in the context of a forward-deployed ballistic missile defense (BMD) radar designed to detect and track targets over 1000 km away.

1.   Forward-Deployed Ballistic Missile Defense

The Navy's key and enduring role lies in its core capability of continuous forward deployment of sovereign U.S. warships. The introduction of BMD into the fleet enables the Navy to project defense ashore from the sea. The result will be a BMD umbrella for expeditionary air and land forces as they move into theater – an increasingly crucial requirement as decreased shore-based presence overseas results in more forces having to deploy into theater from the U.S. in times of crisis. Navy BMD will reduce the asymmetric threat from theater ballistic missiles armed with chemical and biological warheads – reassuring enduring and emerging allies that they are protected too. These ship-based systems have the potential to form the nucleus of the Navy's contribution to a future national missile defense architecture.

2.   The Aperstructure and Opportunistic Array Concepts

The aperstructure concept aims to exploit the entire ship's structure as a radar aperture and employ individual antenna elements that are conformal and integrated into the ship's structure. The opportunistic array concept aims to implement this with an integrated ship-wide digital phased array, where antenna elements are placed at available open areas over the entire length of the ship. Figure 1 illustrates a DD(X)-sized ship with

1200 elements randomly distributed on its top-side structures. A key aspect of the radar architecture is modularity – every element is a self-standing transmit/receive (T/R) module that has no hardwire connections other than power.
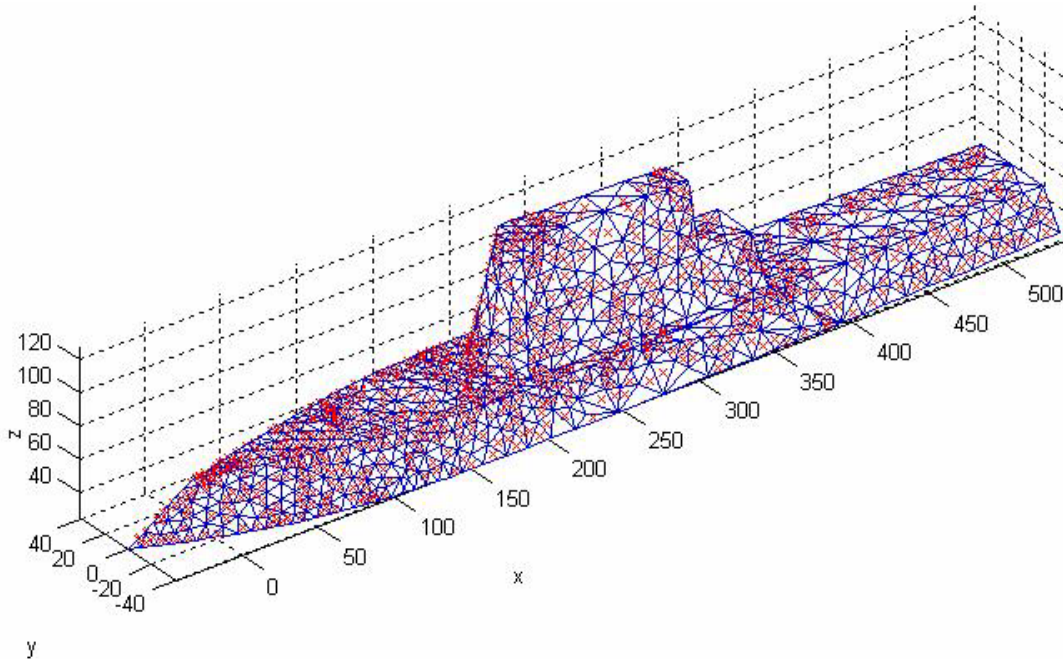
Figure 1   CAD Model of DD(X)-sized Ship with 1200 Randomly Distributed Antenna Elements (A red 'x' denotes an element location).

Such an array has the potential to fulfill many of the Navy's missions, in particular BMD where the radar mission encompasses exo-atmospheric surveillance, tracking and preliminary discrimination. The advantages of aperstructures and opportunistic arrays are discussed in the following paragraphs.

a.   *High Angular Resolution*

The primary advantage of aperstructures and opportunistic arrays is the high angular resolution they can achieve by utilizing the entire ship's structure as an aperture. Angular resolution is the minimum angular separation between two targets at which they can be distinguished. High angular resolution is especially important in BMD applications when it is critical for the radar to detect the exact number of hostile missiles in flight and to track them precisely – at ranges beyond 1000 km.

Angular resolution is proportional to beamwidth. The 3-dB beamwidth, θ_B, of an aperture can be estimated by

$$\theta_B \approx \frac{\lambda}{L} \qquad (1.1)$$

where λ is the wavelength and L is the length of the aperture. Consider a DD(X)-sized ship with a length of approximately 200 m. If the entire ship's structure is exploited as an aperstructure, an opportunistic array operating at 300 MHz will produce a beamwidth on the order of 0.005 radians or $0.3°$. The proposed Cobra Gemini has an expected beamwidth of $1.24°$ [3].

b. Enhanced Stealth

Low profile patch antennas integrated into the ship's structure using hull appliqués hold the key to minimizing the ship's visual and infrared (IR) signatures as well as radar cross section (RCS).

c. Multifunction

The digital architecture of the opportunistic array offers several advantages over conventional radar designs. Advanced signal processing techniques coupled with broadband patch antenna designs offer the possibility of integrating radar, direction finding and satellite communications functions into the array. The result is a single aperstructure replacing the numerous antennas and masts populating the superstructures of present day ships.

d. Increased Survivability and Operational Availability

Opportunistic arrays are inherently more survivable and have increased operational availability vis-à-vis conventional radars. A radar architecture with hundreds of dispersed antenna elements ensures that operations will continue even if a number of elements are disabled – due to enemy action or maintenance requirements. The modularity and accessibility of the antenna elements also means that damaged elements can be quickly replaced, even if the ship is in the high seas. In addition, the relationship between the performance of the radar and the number of functioning elements can be well-predicted, allowing any degradation in radar performance to be compensated by tactical means.

e. *Right Cost*

The digital radar architecture leverages on commercial-off-the-shelf (COTS) technology to achieve high performance at low costs. Moreover, it eliminates the need to maintain several distinct radar and communication systems by integrating their functions.

3. Other Possibilities for Aperstructures and Opportunistic Arrays

The inherent advantages of opportunistic arrays, such as stealth, high angular resolution, multifunction, increased operational availability, low cost and, most importantly, their opportunistic nature, make them excellent candidates for a wide variety of applications.

a. *Other Military Applications*

The opportunistic and modular natures of these arrays can be exploited by the Army or Air Force to rapidly deploy networks of land-based radars in crisis areas. Existing buildings can form the "aperstructures" and, with proper planning, the entire system could be set up under the cover of night. Such hastily formed radar networks can then be used for communications and/or to detect and track targets such as missiles, aircraft or artillery rounds. The fact that these arrays are dispersed, capable of operating under degraded conditions and quickly repaired make them highly resilient to attacks, even from anti-radiation missiles or artillery barrages.

b. *Commercial Applications*

The increased operational availability, multifunction and low costs possibilities of the opportunistic arrays make them commercially attractive. Once the technology is mature, these arrays may be designed for air traffic control at major airports or satellite communication within urban centres.

c. *Disaster Relief*

In the aftermath of the tsunami on 26 December 2004, one of the biggest hurdles to bringing aid to the disaster areas was the lack of air traffic control facilities and communication links. Airports and airstrips existed in several of the affected areas but the lack of air traffic coordination hampered humanitarian efforts and increased the risk faced by aircrafts and their crews. The absence of satellite communication links in places like Aceh Province in Indonesia resulted in many difficulties in the coordination of relief

efforts. Opportunistic arrays offer a robust and flexible solution in such scenarios. Air traffic control and communication links can be quickly established by populating existing buildings with easily transportable modular antenna elements and using these buildings both as "aperstructures" as well as air traffic control and communication centers.

B. PREVIOUS WORK

This thesis continues the design and development of a three-dimensional 2.4 GHz digital phased array radar started in [4] and continued in [5] and [6]. Thus far, a phased array transmit antenna has been designed and built using COTS products. The antenna was used to demonstrate that the genetic algorithm program and its pattern builder function formed a radiation beam in agreement with theoretical calculations. The bandwidth characteristics of COTS products such as the Analog Devices AD8346EVAL Quadrature Modulator board and AD8347EVAL Demodulator board were investigated for suitability of implementation.

C. SCOPE AND ORGANIZATION

1. Scope

This thesis first performs a system-level tradeoff study to investigate the relationship between the number of elements and the radar's theoretical maximum range. The MATLAB programs "ArrayPatternSub.m" and "arraygainSub.m" were used to compute the radiation patterns and gain achieved for various numbers of randomly distributed antenna elements.

Next, the thesis focused on designing a low-profile, broadband U-slot microstrip patch antenna. Theoretical calculations and parametric studies were performed to develop an antenna element that could operate in the upper VHF/lower UHF frequencies. A set of simple design procedures was developed to provide approximate rules that result in a good "first-pass" design with prescribed characteristics that require minimal tuning.

2. Primary Research Questions

This thesis addresses two primary research questions in the development of the aperstructure and opportunistic array concept.

a. Can a ship-based opportunistic array achieve the adequate BMD detection ranges, given the real constraints such as power? And if so, how many elements are needed?

b. Is it possible to design a low-profile integrated conformal patch antenna with broadband characteristics necessary for radar and communication functions?

3. Organization

Chapter II develops the opportunistic array theory, beginning from the basic antenna performance parameters and conventional phased array radar theory to extrapolating the theory of random and thinned arrays. Digital beamforming for the opportunistic array is discussed and a model for predicting the theoretical maximum range of the opportunistic array is developed.

Chapter III discusses the features, advantages and limitations of microstrip patch antennas and illustrates the topology of the U-slot antenna investigated in this thesis. The key considerations in substrate selection as well as the effects of substrate permittivity on the patch antenna's performance are presented. Two published design approaches for the U-slot patch antenna are compared and a hybrid method is developed.

Chapter IV presents the analysis objectives and procedures and discusses the findings of the system study of the aperstructure and opportunistic array concepts. Statistical and numerical methods are used to determine the average sidelobe level and main lobe gain for broadside and endfire configurations. The performance of the radar vis-à-vis the number of antenna elements is investigated.

Chapter V presents the design objectives and procedures for the U-slot microstrip patch antenna. The accuracy of CST Microwave Studio is validated by comparing its results for a U-slot topology with published experimental and computed results. The choices for substrate and coaxial feed are also discussed. The relationships between the U-slot geometry and the impedance characteristics of the patch are investigated parametrically. The proposed design procedures are used to create an initial design which is subsequently optimized using the proposed tuning technique.

Chapter VI discusses the conclusions made in this thesis and recommends objectives for follow-on research.

THIS PAGE INTENTIONALLY LEFT BLANK

II. DEVELOPMENT OF OPPORTUNISTIC ARRAY THEORY

A. ANTENNA PERFORMANCE PARAMETERS

The opportunistic array theory leverages on the depth of radar research conducted since the 1930s and is enabled by the rapid evolution of high performance computers and high speed wireless communication. The performance parameters used to evaluate the opportunistic array, however, is no different from the parameters for conventional dish or phased array radars. A description of these antenna performance parameters, as referenced from [7], follows.

1. Radiation Pattern

The radiation pattern is the angular variation of radiation around the antenna. This thesis discusses two instances of radiation patterns. The first is the radiation pattern created by the entire opportunistic array and aperstructure. The pattern was plotted in MATLAB using the "ArrayPatternSub.m" code and is presented in Chapter IV. The second is the radiation pattern from an individual antenna element. This pattern was developed through simulations run on CST Microwave Studio and is presented in Chapter V.

2. Directive Gain ($D(\theta,\phi)$)

Directive gain is defined as the ratio of radiation intensity in the direction (θ,ϕ) to the radiation intensity averaged over all directions. In mathematical form, directive gain can be written as [7]:

$$D(\theta,\phi) = 4\pi \frac{U(\theta,\phi)}{P_{rad}} \tag{2.1}$$

where

$U(\theta,\phi)$ = radiation intensity in the direction defined by θ and ϕ [W/steradian]

P_{rad} = total radiated power [W]

or

$$D(\theta,\phi) = \frac{U_{max}|F(\theta,\phi)|^2}{U_{average}} = D_{max}|F(\theta,\phi)|^2 \qquad (2.2)$$

where

U_{max} = maximum radiation intensity [W]

$U_{average}$ = average radiation intensity [W]

$|F(\theta,\phi)|^2$ = normalized power pattern in the direction $(\theta_{max},\phi_{max})$

D_{max} = maximum value of directive gain

The maximum value of $D(\theta,\phi)$, is called the directivity, D_{max}. Equation (2.1) is used in the "arraygainSub.m" code to compute the directive gain of the opportunistic array numerically.

3.　　**Gain ($G(\theta,\phi)$)**

The gain of the antenna is closely related to the directivity but accounts for the efficiency of the antenna as well as its directional characteristics. The absolute gain of an antenna in a given direction is defined in [8] as "the ratio of the intensity, in a given direction, to the radiation intensity that would be obtained if the power accepted by the antenna were radiated isotropically. The radiation intensity corresponding to the isotropically radiated power is equal to the power accepted (input) by the antenna divided by 4π". Typically, gain refers to the maximum value of $G(\theta,\phi)$. Mathematically, gain can be expressed as:

$$G(\theta,\phi) = 4\pi\frac{U(\theta,\phi)}{P_{in}} = 4\pi\eta\frac{U(\theta,\phi)}{P_{rad}} = \eta D(\theta,\phi) \qquad (2.3)$$

where

P_{in} = total input power [W]

η = antenna efficiency $(0 \le \eta \le 1)$

Alternatively, gain can be expressed as:

$$G(\theta,\phi) = \frac{4\pi A_e}{\lambda^2} |F(\theta,\phi)|^2 \qquad\qquad (2.4)$$

where

A_e = effective area of aperture [m^2]

λ = wavelength [m]

Equation (2.2) is used in Chapter IV to compare the theoretical and numerically determined values of gain.

4. Polarization

The polarization of an antenna is the polarization of wave transmitted by the antenna. Possible polarizations of the wave (and hence the antenna) include linear, circular and elliptical. The polarization of the array has not been finalized but most likely will be linear and vertical.

5. Impedance (Z_A)

The impedance refers to the input impedance at the antenna terminals. In this thesis, the input impedance of the antenna was designed to be 50 Ω, a common transmission line value.

6. Bandwidth

The bandwidth of an antenna is defined as the range of frequencies within which the performance of the antenna, with respect to specific characteristics, conforms to a specified standard. The desired bandwidth for this application was specified as 20% based on the return loss values below -10 dB. (Return loss is a measure of the reflection coefficient at the antenna terminals.)

7. Scanning

Scanning refers to the movement of the radiation pattern main beam in space. Scanning can be accomplished by mechanical movement or by electronic means such as adjustment of current phase to individual antenna elements. The aperstructure and opportunistic array concept uses the latter method.

8. System Considerations

System considerations include size, weight, power requirements, radar cross section and environmental operating conditions, among others. This thesis focuses on

studying the size and power requirements needed to achieve a radar theoretical maximum range of at least 1000 km.

B.   CONVENTIONAL PHASED ARRAY RADARS

Phased array antennas are typically formed by multiple single-element antennas spatially distributed in two- or three-dimensions. The radiation pattern or field of view (FOV) of a single-element is typically wide, with low values of directivity (or gain). The radiation pattern of a phased array, however, is the vector addition of the radiation patterns of individual elements and can achieve very directive characteristics. In an array of identical elements, there are five factors that can be used to shape the overall radiation pattern of the antenna [9]:

1.   Geometrical configuration of the overall array.

2.   Relative displacement between elements.

3.   Excitation amplitude of the individual elements.

4.   Excitation phase of the individual elements.

5.   Relative pattern of the individual elements.

Arrays offer several advantages over aperture antennas. The main beam is electronically steered and hence the scan rate is limited primarily by the speed of the control electronics. As a result, arrays are able to track multiple targets quickly. Arrays can also be made up of conformal antenna elements that integrate into the structures of ships and aircraft, thus reducing their aerodynamic drag as well as visual, infrared and radar signatures. The disadvantages of arrays, however, include complex circuitry and signal processing.

1.   Array Factor (*AF*)

In most cases, the total field of an array can be determined by multiplying the field of a single element positioned at the origin with a factor called the array factor. This assumes identical element patterns. The array factor is primarily a function of the geometry of the array and the excitation phase, among other parameters. A linear array can be used to illustrate the derivation of the array factor. Consider the linear array of N

uniformly spaced identical isotropic elements shown in Figure 2. The individual antenna elements are phased to produce a wave propagating at an angle θ relative to the z-axis.
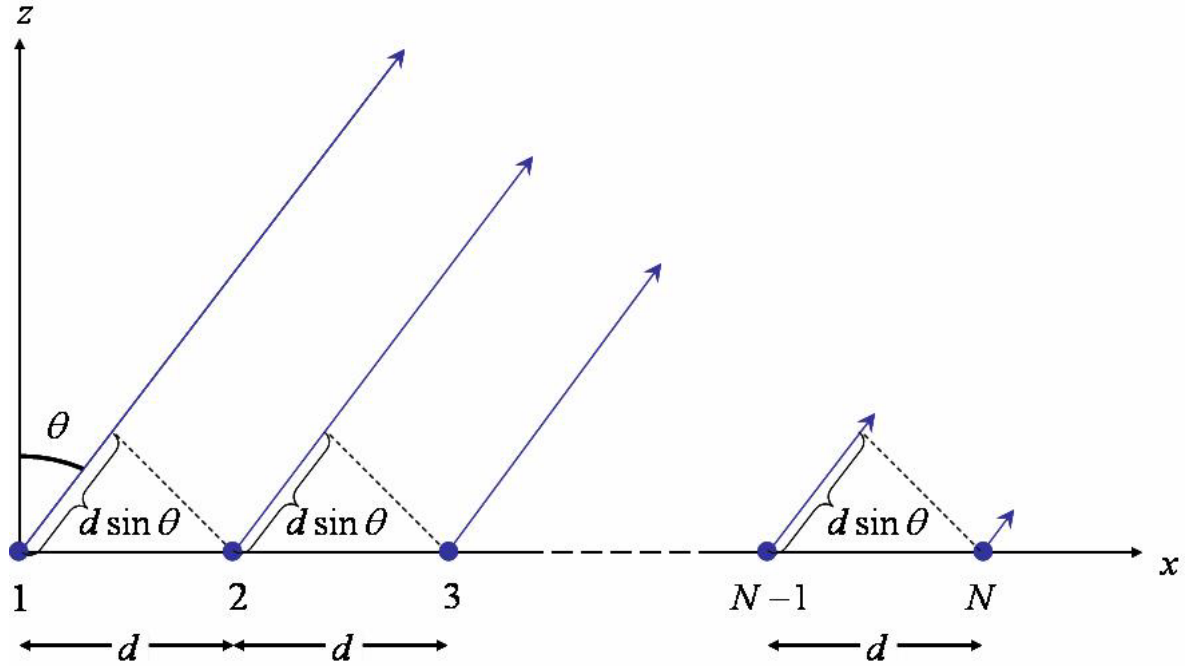
Figure 2 Linear Array of N Uniformly Spaced Identical Isotropic Antenna Elements (After Ref. [9]).

Every antenna element is separated by a distance d from neighboring antenna elements. All the elements have identical amplitudes, but the nth element has a progressive lead phase Φ_n relative to the preceding one. This lead phase Φ_n is used to properly phase each antenna element in order to form and steer the main beam. If all the elements are also assumed to be point sources, the array factor, AF, is given by:

$$
\begin{aligned}
AF &= 1 + e^{+j(kd\sin\theta+\Phi_2)} + e^{+j2(kd\sin\theta+\Phi_3)} + \cdots + e^{+j(N-1)(kd\sin\theta+\Phi_N)} \\
&= \sum_{n=1}^{N} e^{+j(n-1)(kd\sin\theta+\Phi_n)} \\
&= \sum_{n=1}^{N} e^{+j\Phi_n} e^{+j(n-1)(kd\sin\theta)}
\end{aligned}
\tag{2.5}
$$

Since the total array factor for the uniform array is a summation of complex exponentials, it can also be represented by the vector sum of N phasors – each of unit amplitude and progressive lead phase Φ_n relative to the previous one. This is illustrated in Figure 3.
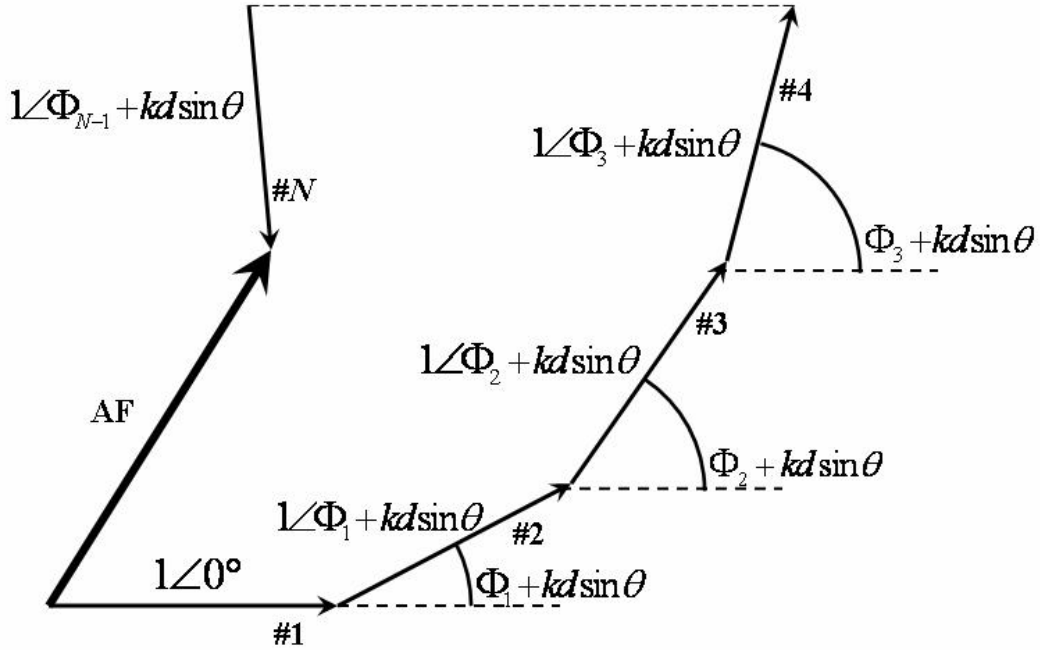
Figure 3   Phasor Representation of Array Factor for Linear Array of N Uniformly Spaced Identical Isotropic Antenna Elements (After Ref. [9]).

The phasor diagram indicates that the amplitude and phase of the array factor can be controlled by changing the relative phase Φ_n between the elements. By extrapolating this idea, it is deduced that the array factor for arrays with unequal spacing between elements can be controlled by changing both amplitude and phase of each element.

2.   Inherent Disadvantages of Periodic Phased Arrays

Phased array radars are most commonly designed as periodic arrays.   In developing the aperstructure concept, however, it is important investigate if aperiodic arrays are able to achieve comparable performance.   This is because the ship's superstructure makes it physically unfeasible to implement a uniform, periodic array over the entire ship's structure.   In addition, integrating an array of closely spaced antenna elements across the entire ship's structure is impractical and likely to be extremely costly.

Periodic array designs typically maximize the spacing between individual antenna elements yet keep it small enough to eliminate grating lobes. The condition for avoiding grating lobes under all conditions of beam-steering as discussed in [11] is:

$$d \leq \frac{\lambda}{2} \tag{2.6}$$

This condition requires antenna elements to be closely spaced and results in two inherent disadvantages.

a. High Cost of Large Periodic Arrays

The cost of phased array systems is approximately proportional to the number of elements in the array. For a linear array of length L with N periodic elements,

$$L = N \times d \approx \frac{N\lambda}{2} \tag{2.7}$$

The 3-dB beamwidth θ_B is proportional to the angular resolution and is given by Equation (1.1). Note that the 3-dB beamwidth is a function of the length and not the number or distribution of the individual antenna elements. Combining the Equations (1.1) and (2.7) derives the relationship between the number of elements (and hence array cost) and angular resolution.

$$N \approx \frac{2}{\theta_B} \tag{2.8}$$

Observe that the cost of a linear and periodic phased array increases as the reciprocal of the desired angular resolution. In a two-dimensional array, both the number of elements and the cost will increase as the square of the desired angular resolution. As a result, the cost of large periodic arrays can be prohibitive. Hence, it makes economic sense to study and explore the use of thinned and aperiodic arrays as a means of reducing costs (and weight) vis-à-vis large periodic arrays.

b. Mutual Coupling

Mutual coupling occurs between closely spaced antenna elements. Coupling may occur by radiation, from surface paths, from paths within the feed structure or from reflections at the antenna terminal due to impedance mismatches. The effects of

15

mutual coupling include distortions in the radiation pattern and variations in the element gains. Mutual coupling may be characterized by a coupling coefficient c_{mn} that relates the current flowing into the nth element due to the current from the mth element. For isotropic elements, this coefficient is given in [11] as:

$$c_{mn} = \frac{\sin(kd_{mn})}{kd_{mn}} \qquad (2.9)$$

where d_{mn} is the distance between n^{th} and m^{th} elements.

Figure 4 graphs the relationship between the mutual coupling coefficient and the separation between antenna elements. Observe that Equation (2.9) is simply a sinc function. Hence, the effects of mutual coupling are undulatory with the distance between the elements with the envelope of the coupling coefficient decreasing with separation.
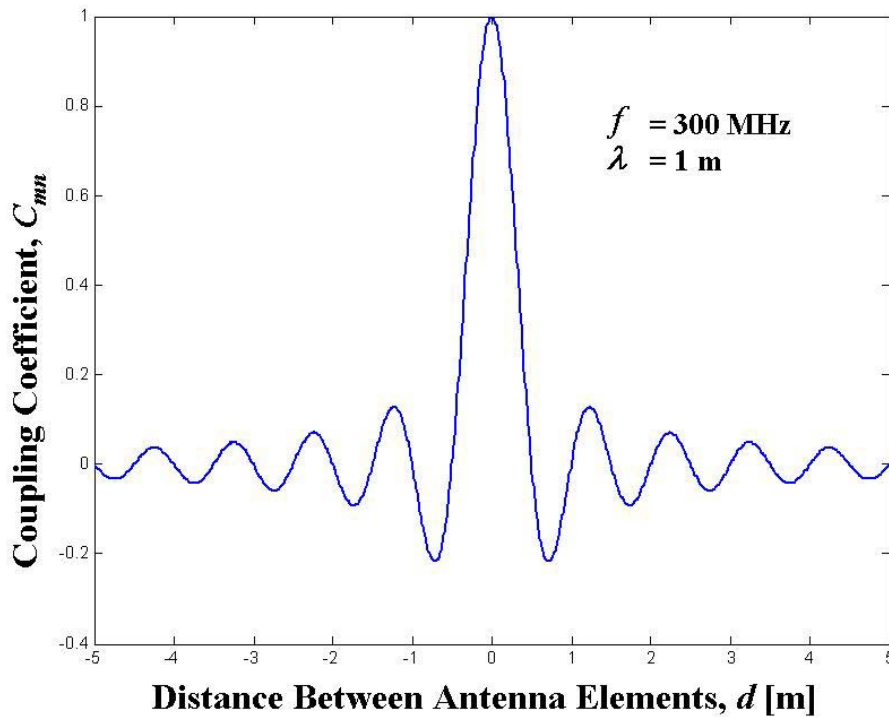
Figure 4   Relationship between Mutual Coupling Coefficient and Separation of Antenna Elements.

Theoretically, the effects of mutual coupling can be calculated and hence compensated. In reality, the coupling coefficient is not easily measured, is not stable with scan angle and is not conveniently controlled – especially for large ship-sized arrays which are too big to be tested in a controlled environment.

The best way to reduce the effects of mutual coupling is to increase the distance between individual antenna elements beyond the requisite $\frac{\lambda}{2}$ criteria presented in Equation (2.6). This process is commonly known as "thinning". This approach, however, can result in higher sidelobes and increased grating lobes levels unless an aperiodic array is designed.

C. RANDOM ARRAYS

Random arrays can be described as aperiodic, thinned arrays. Random arrays are of particular interest in the development of the aperstructure and opportunistic array concepts for two reasons. Firstly, the opportunistic array will be thinned and aperiodic by design as the presence of the ship's superstructure as well as the size of the ship make it physically unfeasible for antenna elements to be closely spaced and periodic. Secondly, in rare circumstances, individual antenna elements on the aperstructure could fail. The locations of the failed antenna elements will be random – in effect thinning the array randomly. The following paragraphs combine analytical and statistical approaches to discuss two critical parameters of random arrays.

1. Array Factor for Random Arrays (AF)

Figure 5 illustrates a linear array of N randomly spaced identical isotropic elements. Note that Figure 5 is similar but not identical to Figure 2. The antenna elements are separated by a random distance d_n. All the elements have identical amplitudes but the nth element has a progressive lead phase Φ_n relative to the preceding one. This lead phase Φ_n is used to properly phase each antenna element in order to form and steer the main beam. If all the elements are also assumed to be point sources, the array factor for the random array, AF, is given by:

$$AF = 1 + e^{+j(kx_2 \sin\theta + \Phi_2)} + e^{+j(kx_3 \sin\theta + \Phi_3)} + \cdots + e^{+j(kx_N \sin\theta + \Phi_N)}$$

$$= \sum_{n=1}^{N} e^{+j(kx_n \sin\theta + \Phi_n)} \qquad (2.10)$$

$$= \sum_{n=1}^{N} e^{+j\Phi_n} e^{+j(kx_n \sin\theta)}$$

where

$$x_1 = 0$$
$$x_2 = d_2$$
$$x_3 = d_2 + d_3$$
$$\vdots$$
$$x_N = d_2 + d_3 + \cdots + d_N$$

Again, this derivation is similar but not identical to the derivation of Equation (2.5).
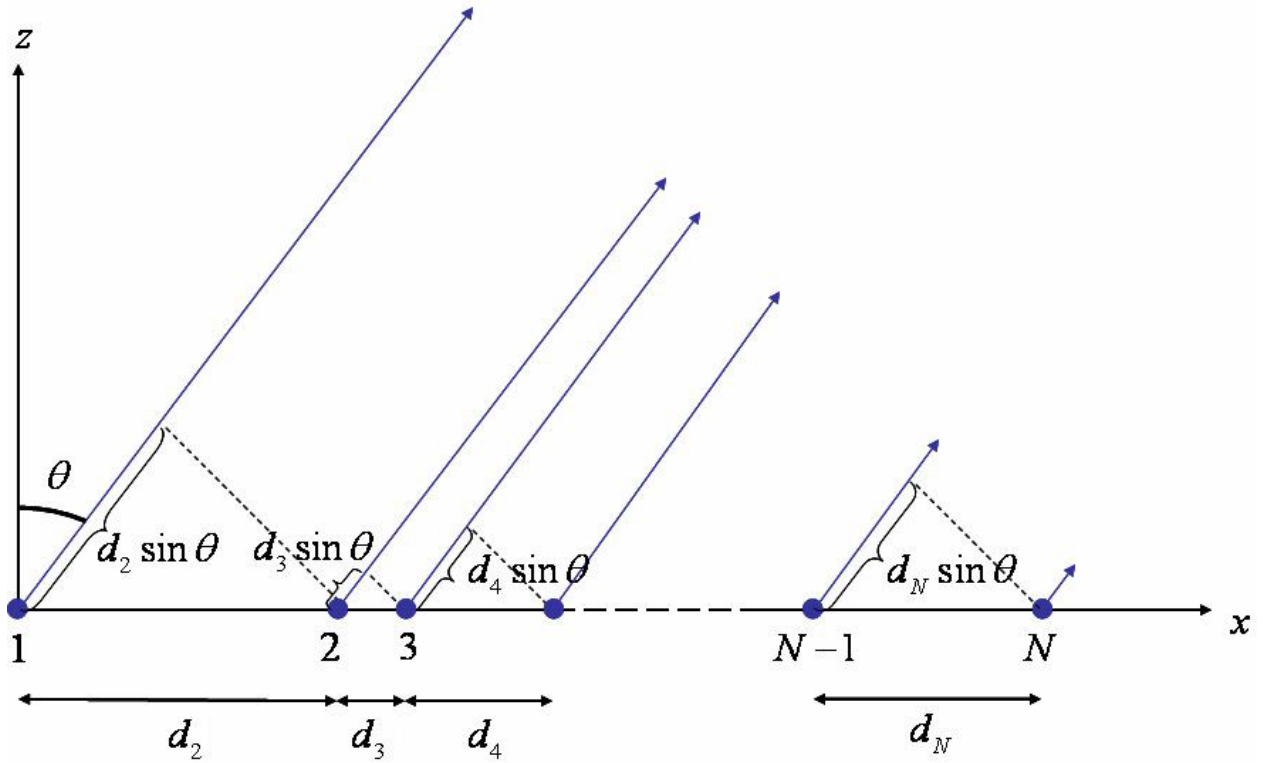
Figure 5   Linear Array of N Randomly Spaced Identical Isotropic Elements.

18

2.   Average Sidelobe Level vs. Number of Elements, N

Without loss of generality, assume that the array is properly phased to form the main lobe perpendicular to the array (a broadside scan condition). Figure 6 shows the phasor diagram representing the array factor for N randomly spaced antenna elements.
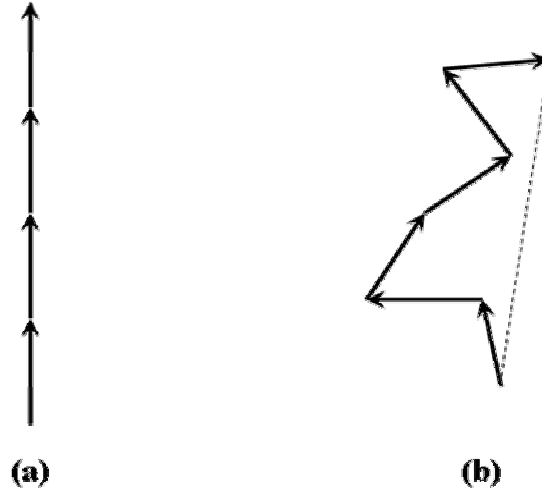
Figure 6   (a) Phasor Diagram for N Randomly Spaced Elements Forming the Main Lobe. (b) Phasor Diagram for N Randomly Spaced Elements Forming a Sidelobe (After Ref. [10]).

Note that from Equation (2.10) the main lobe amplitude is N, occurring when all antenna elements are properly phased (i.e. $\Phi_n = -kx_n \sin\theta$ for all elements). For the sidelobes, however, the phase angle $kx_n \sin\theta$ is a random variable because the element location, represented by x_n is a random variable. As a result, the root-mean-square (RMS) amplitude of the sidelobes increases as $\sqrt{N}$.

Since power is determined by the square of the array factor and hence the square of the amplitude, the ratio of the average sidelobe power, $P_{sidelobe}$, to the main lobe power, $P_{mainlobe}$, can be derived as follows.

$$\frac{P_{sidelobe}}{P_{mainlobe}} = \left(\frac{\sqrt{N}}{N}\right)^2$$

$$= \frac{N}{N^2} \tag{2.11}$$

$$= \frac{1}{N}$$

In decibels, this ratio is $10\log_{10}\left(\frac{1}{N}\right)$.

3.   Average Power Pattern vs. Number of Elements, N

The power pattern of an array can be determined by the product of the array factor (which is a voltage or electric field quantity) and its complex conjugate. Consider the expression for the array factor of N randomly spaced linear elements given in Equation (2.10). Without loss of generality, assume that the array is properly phased to form the main lobe perpendicular to the array. As a result, $\Phi_n = 0$ and $e^{+j\Phi_n} = 1$ for all elements. Let $u = \sin\theta$, transforming Equation (2.10) to the following form:

$$AF = \sum_{n=1}^{N} e^{+jkx_n u} \tag{2.12}$$

Following the derivation in [11], the expected power pattern, $\overline{P}$, can be expressed as:

$$\overline{P} = \overline{AF \times AF^*}$$

$$= \frac{1}{N^2}\overline{\sum_{n}^{N}\sum_{m}^{N} e^{+jk(x_n-x_m)u}} \tag{2.13}$$

where the overbar is the expectation operator. Since the average of a sum equals the sum of the averages,

$$\overline{P} = \frac{1}{N^2}\sum_{n}^{N}\sum_{m}^{N}\overline{e^{+jk(x_n-x_m)u}}$$

$$= \frac{1}{N^2}[N + \overline{e^{+jkxu}}\,\overline{e^{-jkxu}}(N^2-N)]$$

$$= \frac{1}{N^2}[N + \overline{AF}\,\overline{AF^*}(N^2-N)] \tag{2.14}$$

$$= \left|\overline{AF}\right|^2(1-\frac{1}{N}) + \frac{1}{N}$$

20

The relationship between the expected power pattern and the number of antenna elements derived above consists of two terms. The first term is the desired power pattern. The second term is an additive, angle-independent term of strength $\frac{1}{N}$. It is the quantity established in Equation (2.11) as the ratio of the mean sidelobe level to the main lobe. Hence, the relationship between the expected power of the main lobe, $\overline{P}_{mainlobe}$, and the number of antenna elements is

$$\overline{P}_{mainlobe} = \left|\overline{AF}\right|^2 \left(1 - \frac{1}{N}\right) \tag{2.15}$$

4. Expected Gain vs Number of Elements, N

The MATLAB programs "ArrayPatternSub.m" and "arraygainSub.m" derive the gain of the aperstructure, not the power of the main lobe. Hence, the relationship between the gain and the expected power of the main lobe must be determined. The normalized power pattern of a random array can be determined by normalizing Equation (2.15).

$$\left|F(\theta,\phi)\right|^2 = \frac{\left|\overline{AF}\right|^2 \left(1 - \frac{1}{N}\right)}{\left|\overline{AF}\right|^2} \tag{2.16}$$
$$= 1 - \frac{1}{N}$$

Combining Equations (2.4) and (2.16) gives

$$G(\theta,\phi) = \frac{4\pi A_e}{\lambda^2}\left(1 - \frac{1}{N}\right) \tag{2.17}$$

Since the effective area of the aperture, A_e, is proportional to the number of elements, N, the relationship between the expected gain and the number of elements is

$$G(\theta,\phi) \propto N\left(1 - \frac{1}{N}\right) \tag{2.18}$$
$$\propto N - 1$$

21

D. DIGITAL BEAMFORMING FOR OPPORTUNISTIC ARRAYS

The opportunistic array is really an implementation of a random array. In this section, a numerical approach is developed to study the characteristics of the opportunistic array instead of the probabilistic approach of the previous section. In Chapter IV, the results derived through the numerical approach are compared with the expected results determined through the probabilistic approach.

1. Array Factor

Figure 7 shows the coordinate system referenced to a DD(X)-sized ship. A more general form of the array factor in three-dimensions for elements located at (x_n, y_n, z_n) for $n = 1, 2, 3, \ldots, N$ is

$$AF(\theta, \phi) = \sum_{n=1}^{N} A_n e^{+j\Psi_n} e^{+j\vec{k} \bullet \vec{r}_n} \tag{2.19}$$

where

$A_n e^{+j\Psi_n}$ = complex coefficient of the nth element that accounts for beam scanning, sidelobe control and corrections for all hardware non-idealities.

Ψ_n = $-k\left[(\sin\theta_S \cos\phi_S)x_n + (\sin\theta_S \sin\phi_S)y_n + (\cos\theta_S)z_n\right]$

(θ_S, ϕ_S) = scan angle as shown in Figure 7

$\vec{k}$ = $k(\hat{x}\sin\theta\cos\phi + \hat{y}\sin\theta\sin\phi + \hat{z}\cos\theta)$

$\vec{r}_n$ = position vector to element n

  = $\vec{r}_n = \hat{x}x_n + \hat{y}y_n + \hat{z}z_n$

22
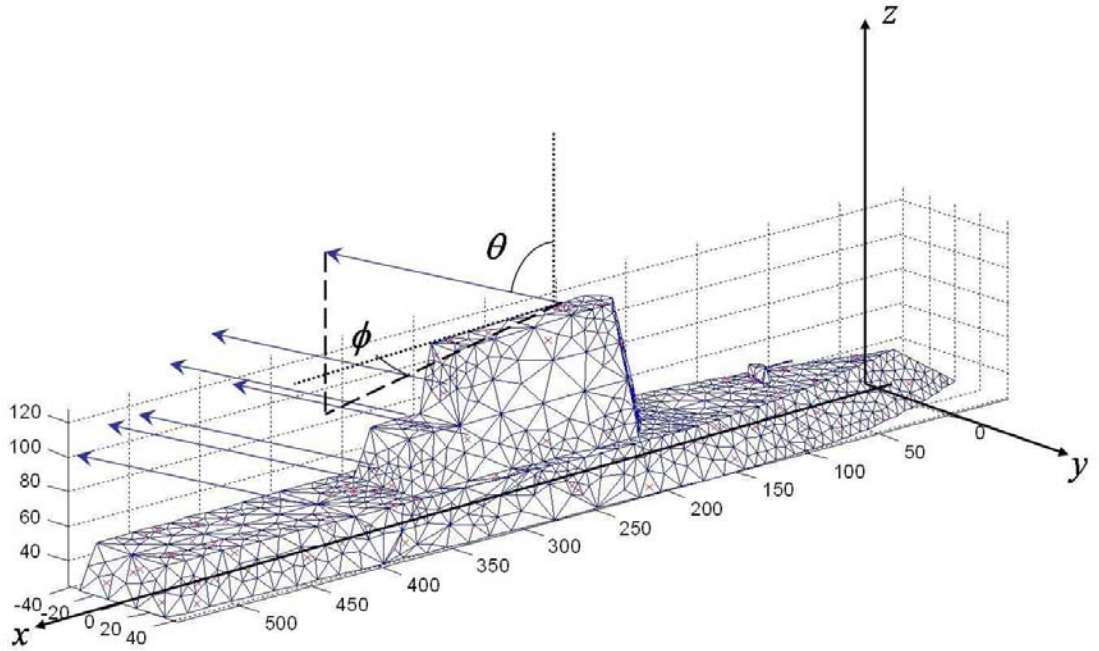
Figure 7   Spherical Coordinate System Referenced to DD(X)-sized Ship.

In the case of a distributed array, however, it is possible that flexing of the ship will produce errors in the locations of the antenna elements. The position vector to element n then becomes:

$$\vec{r}_n = (x_{0n} + \Delta x_n)\hat{x} + (y_{0n} + \Delta y_n)\hat{y} + (z_{0n} + \Delta z_n)\hat{z}$$
$$= \vec{r_{0n}} + \vec{\Delta r_n}$$

(2.20)

where

(x_{0n}, y_{0n}, z_{0n}) = error-free element location

$(\Delta x_n, \Delta y_n, \Delta z_n)$ = deviation from the error-free location

23
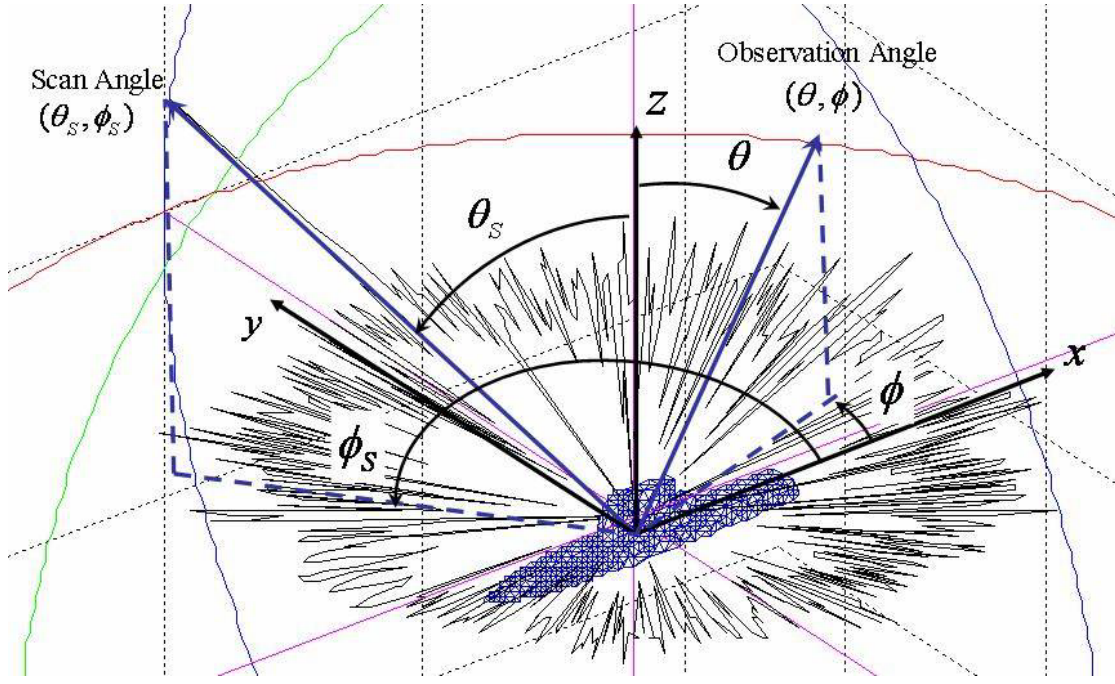
Figure 8   Illustration of Scan Angle (θ_S, ϕ_S) and Observation Angle (θ, ϕ).

2.   Element Factor

The element factor is the pattern of an individual element of the array. For any given direction, only those elements whose FOV are in the scan direction contribute to the main lobe. Elements that do not contribute are turned off while the contributions of the remaining elements are used to determine the array factor. Hence, the element factor can be expressed as:

$$EF_n = \begin{cases} |\hat{n}_n \bullet \hat{r}|, & \hat{n}_n \bullet \hat{r} > 0 \\ 0, & \text{otherwise} \end{cases} \qquad (2.21)$$

where

EF_n = Element factor of the nth element.

$\hat{n}_n$ = Vector normal to the surface of the nth element.

3. Pattern Factor

The pattern factor, $F(\theta, \phi)$, is derived as product of the array factor and the element factor

$$F(\theta, \phi) = \sum_{n=1}^{N} A_n e^{+j\Phi_n} e^{+j\vec{k}\cdot\vec{r}_n} EF_n(\theta, \phi) \qquad (2.22)$$

The pattern factor is used in the programs "ArrayPatternSub.m" and "arraygainSub.m" to determine the radiation pattern of the opportunistic array. The directivity defined in Equation (2.1) can be written in terms of the pattern factor

$$D(\theta, \phi) = \frac{4\pi}{\int_0^{2\pi} \int_0^{\frac{\pi}{2}} \frac{|F(\theta, \phi)|^2}{|F_{max}|^2} \sin\theta \, d\theta \, d\phi} \qquad (2.23)$$

E. PREDICTION OF RADAR RANGE

The radar's theoretical maximum range can be predicted using the radar range equations discussed in [12]. These equations account for many, but not all, of the factors that influence the performance of a noise-limited radar system.

1. Peak Transmit Power Model

The maximum detection range for a radar using a pulse train waveform is given by

$$R_{max}^4 = \frac{P_t G A_e \sigma n E_i(n)}{(4\pi)^2 k_B T_0 B_n F_n (S/N)_1} \qquad (2.24)$$

where

R_{max}	= Maximum radar range or detection range [m]
P_t	= Transmitted power [W]
G	= Antenna gain
A_e	= Antenna effective aperture [m^2]
σ	= Radar cross section of target [m^2]

n = Number of pulses integrated

$E_i(n)$ = Integration efficiency

k_B = Boltzmann's constant = 1.38×10^{-23} [J/degree]

T_0 = Standard temperature = 290 [K]

B_n = Receiver noise bandwidth [Hz]

F_n = Receiver noise figure

$(S/N)_1$ = Signal-to-noise ratio (SNR) required for detection based on a single pulse

In this thesis, however, the average power, P_{av}, is of more interest than the peak transmitter power, P_t. There are two reasons for this. Firstly, the average power is a more useful quantity than the peak power when specifying the power requirements to the ship designers. Secondly, the average power-aperture area product is a major design parameter for search radars [12].

2.   Average Transmit Power Model

The average power of a radar is defined as the average transmitter power over the duration of the total transmission. Assuming that the transmitter waveform is a train of rectangular pulses of width τ and constant pulse-repetition period, $T_p = \dfrac{1}{f_p}$, where f_p is the pulse repetition frequency (PRF), the relationship between the average power and the peak power is:

$$P_{av} = \frac{P_t \tau}{T_p} = P_t \tau f_p \qquad (2.25)$$

Substituting Equation (2.25) into Equation (2.24), the radar range equation becomes

$$R_{max}^4 = \frac{P_{av} G A_e \sigma n E_i(n)}{(4\pi)^2 k_B T_0 F_n (B_n \tau)(S/N)_1 f_p} \qquad (2.26)$$

Equation (2.26) is used in Chapter IV to evaluate the detection range of the aperstructure and opportunistic array concept.

3. Noise Figure of Cascaded Networks

The receiver noise figure, F_n, is the only parameter in the radar range equation that needs further refinement. The aim of the refinement is to evaluate the suitability of the COTS demodulators undergoing concurrent research. The receiver noise figure can be described as a measure of the noise produced by a practical receiver compared to the noise of an ideal receiver, expressed mathematically as:

$$F_n = \frac{N_{out}}{k_B T_0 B_n G} \tag{2.27}$$

where G is the gain of the device. Figure 9 illustrates two networks in cascade, each with the same noise bandwidth but different noise figures and gains.
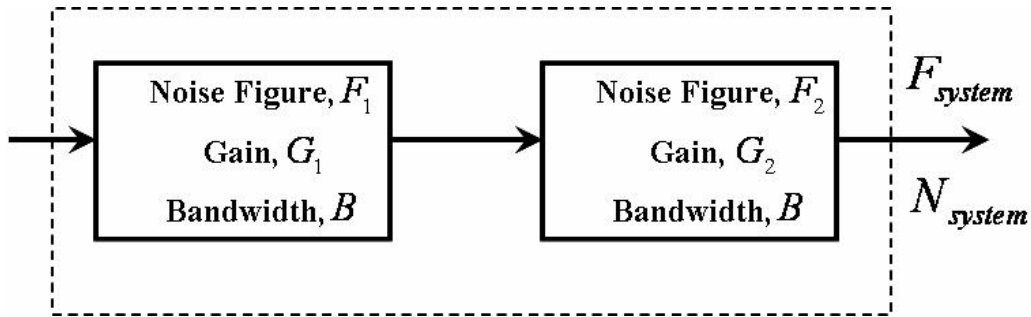
Figure 9   Two Cascaded Networks with Same Noise Bandwidth, Different Noise Figures and Gains (After Ref. [12]).

Following the derivation in [12], the noise figure, F_{system}, of the network system is

$$F_{system} = F_1 + \frac{F_2 - 1}{G_1} \tag{2.28}$$

Expanding this, the noise figure of N devices in cascade may be shown to be

$$F_{system} = F_1 + \frac{F_2 - 1}{G_1} + \frac{F_3 - 1}{G_1 G_2} + \cdots + \frac{F_N - 1}{G_1 G_2 \cdots G_{N-1}} \tag{2.29}$$

Equation (2.29) shows that the cascaded device can be replaced by a single device with noise figure F_{system} and output noise N_{system}.

27

THIS PAGE INTENTIONALLY LEFT BLANK

III. DESIGN OF U-SLOT MICROSTRIP PATCH ANTENNAS

A. COMMERCIAL DEVELOPMENT OF MICROSTRIP PATCH ANTENNAS

In recent years, the rapid evolution of high-speed wireless communication technology coupled with the exponentially increasing demand for high-performance mobile applications have spurred intensive research into broad-band, low-profile antennas. Microstrip patch antennas possess the physical characteristics that make them ideal for mobile phones, Bluetooth personal networks and wireless local networks – simple topologies, compactness and conformality.   Interestingly, these exact characteristics are also desirable in the aperstructure and opportunistic array concepts.

"Classical" rectangular microstrip patch antennas, however, have bandwidths of approximately 2% to 5% – too narrow for use in typical communication systems. Figure 10 shows the topology of a rectangular microstrip patch antenna. Its simplicity – a patch of metallization on a grounded substrate – allows simple analysis and has resulted in well-established theory and analytical models that accurately characterize its behavior. As described later in this thesis, the theory for the rectangular microstrip patch antenna can be leveraged to develop the design guidelines for the U-slot microstrip patch antenna. Figure 11 shows some common feeding methods for the microstrip patch antenna. The third method, using a feed through line with a coaxial probe, will be used in this thesis.
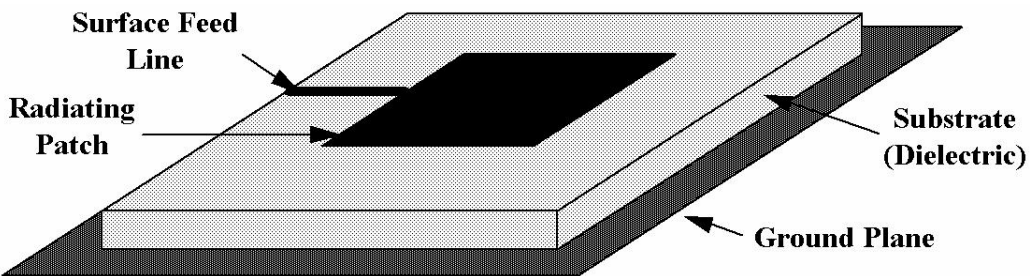
Figure 10   "Classical" Rectangular Microstrip Patch Antenna (After Ref. [13]).

Top View

Proximity Coupling

Surface Line

Feed Through Line
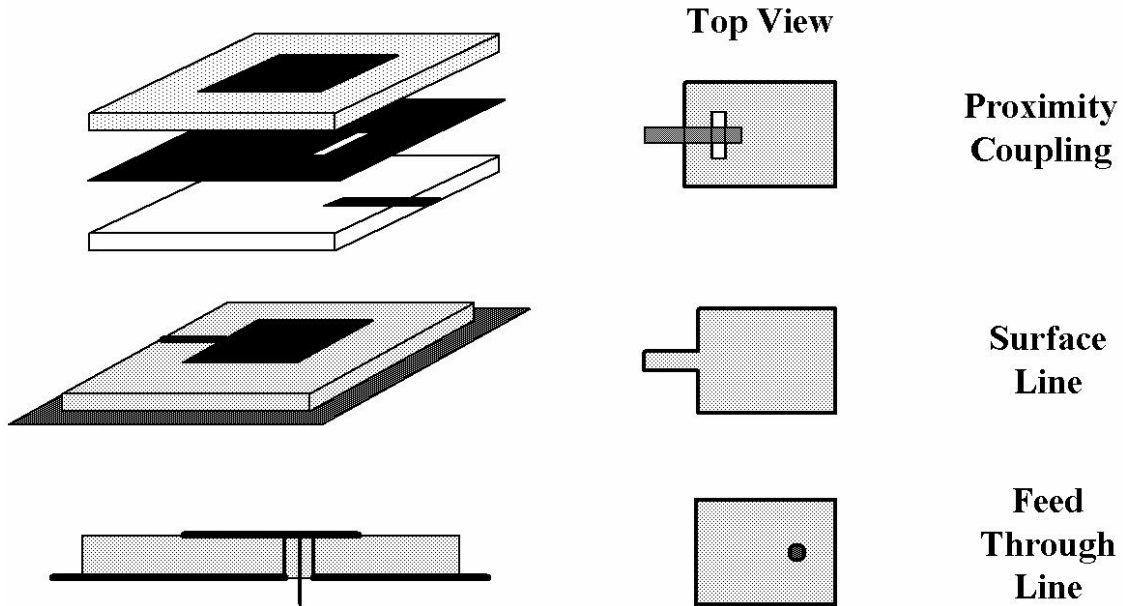
Figure 11   Common Feeding Methods for Microstrip Patch Antennas
(After Ref. [13]).

Many techniques have been devised to increase the bandwidth of microstrip patch antennas. Two simple and common methods are to increase the patch height or decrease the substrate permittivity. Both, however, are typically inadequate as the former quickly nullifies the low-profile advantage of the patch while the latter is subject to material availability and suitability. As described in [14], [15] and [16], more sophisticated techniques include using a stacked patch (a multilayer structure consisting of several parasitic radiating elements with slightly different sizes above the driven element) or a coplanar parasitic subarray (a planar patch antenna surrounded by closely spaced parasitic patches). Both methods, however, obviate the realization of a low-profile, compact antenna element. Another technique of achieving wider bandwidths involves aperture coupled excitations but this method complicates the fabrication process due to the need for complex feed element designs.

There is a technique that can increase the bandwidth while maintaining a low-profile, compactness and a simple topology – modifying the basic element geometry. Figure 12 shows some common patch configurations that can be used to achieve increased bandwidth. The disadvantage of this method, however, is complex analysis. The relationships between the antenna geometries and characteristics are typically too

complex to represent analytically. This technique will be used in this thesis to increase the bandwidth of the U-slot patch.

Folded Dipole **Bow Tie** **Rectangular Slotted**

Circular Slotted **Circular With "Ears"**
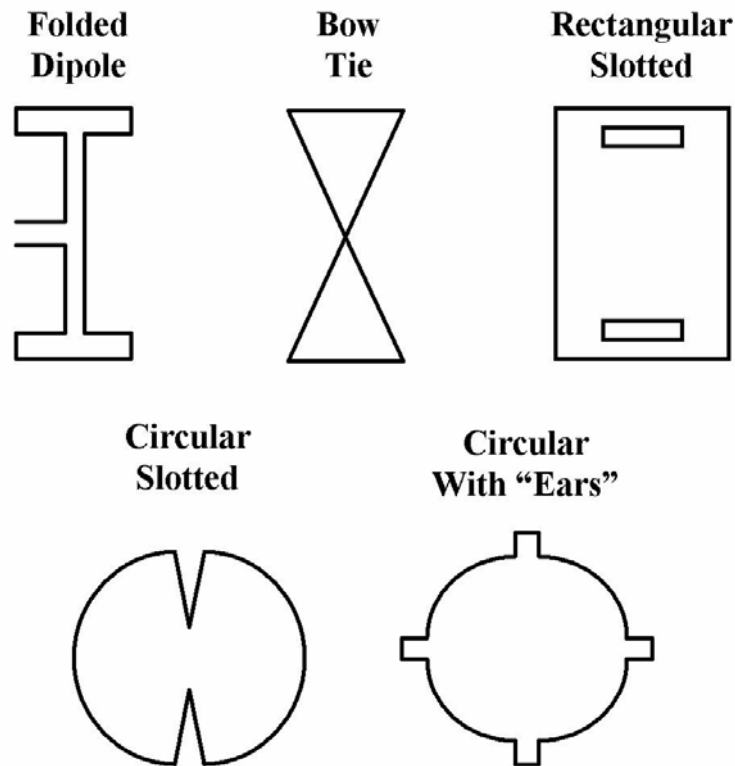
Figure 12   Common Patch Configurations Used to Achieve Increased Bandwidth (After Ref. [13]).

The U-slot antenna element design was first presented in [17] and boasted an impedance bandwidth of 47%. This was a pioneering design because it achieved large bandwidths with a very simple topology – a simple coaxial feed, a simple U-slot patch design and a single layer foam substrate. Since then, many experimental and theoretical studies have been performed on the U-slot antenna design but no accurate analytical models have been developed. As a result, there are no analytical design methodologies available. Two different parametric design approaches, however, have been presented in [18] and [19]. Interestingly, the two approaches produce significantly different designs. The concepts and differences between these two approaches are discussed in Section D of this chapter.

It is important to note that the parametric design procedures described in [18] and [19] were for U-slot microstrip patch antennas operating in between 2 GHz to 6 GHz. The desired frequency range for the aperstructure and opportunistic array concepts, however, is approximately between 200 MHz (upper VHF) to 450 MHz (lower UHF). In developing the U-slot, both methods were evaluated for their performance at the desired frequency range. This thesis proposes a hybrid approach that includes aspects from both [18] and [19] to provide a set of simple design procedures for a low-profile, broad-band, probe-fed U-slot microstrip patch antenna. The computer-aided design (CAD) software CST MICROWAVE STUDIO, developed by Computer Simulation Technology, was used as a simulation tool.

B. ADVANTAGES AND LIMITATIONS OF MICROSTRIP PATCH ANTENNAS

Microstrip patch antennas and arrays are of tremendous commercial interest because of their numerous advantages. These advantages, as discussed in [14], include:

1. Light weight, low volume and conformal configurations.
2. Low fabrication cost.
3. Linear and circular polarizations possible with simple feeds.
4. Dual-frequency and dual-polarization designs possible.
5. No cavity backing required.
6. Compatible with integrated circuits.
7. Feed lines and matching networks can be fabricated simultaneously with the antenna structure.

These advantages that make microstrip patch antennas highly suitable for commercial mobile, high-speed communication applications also make them ideal for the aperstructure and opportunistic array concepts. The limitations of microstrip antennas and arrays, as compared with conventional antennas, are:

1. Narrow bandwidth and associated tolerance problems.
2. Lower gain.
3. Large ohmic loss in the feed structure of arrays.
4. Most microstrip antennas radiate into half-space only.
5. Complex feed structures required for typical high-performance arrays.

6.   Polarization purity hard to achieve.

7.   Excitation of surface waves.

8.   Extraneous radiation from feeds and junctions.

9.   Lower power handling capability (approximately 100 W).

10.   Possibility of reduced gain and efficiency, high levels of cross-polarization and mutual coupling within an array environment at high frequencies.

Nonetheless, some of these limitations can be overcome through specialized techniques. This thesis, for example, investigates incorporating a U-slot into the design to achieve broad-band characteristics as well as using an array configuration to achieve desired gain levels.

C.   TOPOLOGY OF THE RECTANGULAR, PROBE-FED, U-SLOT MICROSTRIP PATCH ANTENNA ON A SINGLE-LAYER, GROUNDED SUBSTRATE

The key advantage of the U-slot design is that it produces broad-band characteristics with a very simple topology. Figure 13 shows the topology of the U-slot microstrip patch antenna investigated in this thesis.

The aim of introducing the U-slot on the rectangular patch is to produce four resonance frequencies [18]. Broad-band operation is achieved when the second and third resonance frequencies are sufficiently close.

Experimentally, it has been shown that variations in parameters such as the width and length of the U-slot, height and size of the patch, probe size and location as well as substrate permittivity can dramatically change the antenna's behavior. To date, no analytical methods have been developed that accurately relate the complex relationships between the antenna dimensions and characteristics. Consequently, no analytical procedures can be offered to determine the dimensions depicted in Figure 13.
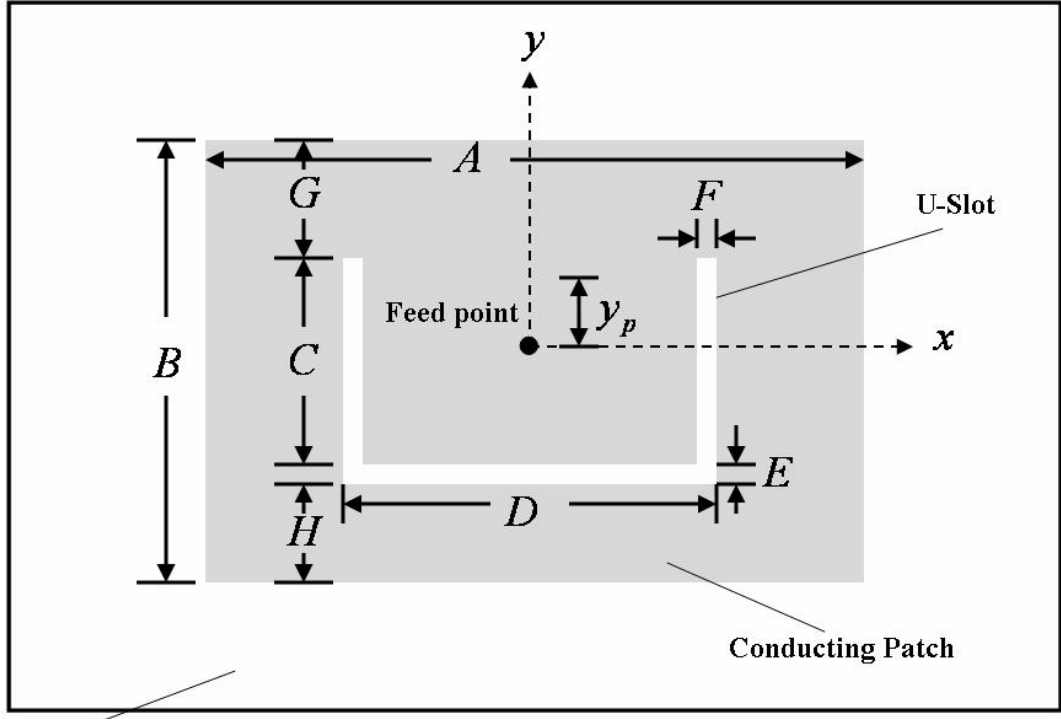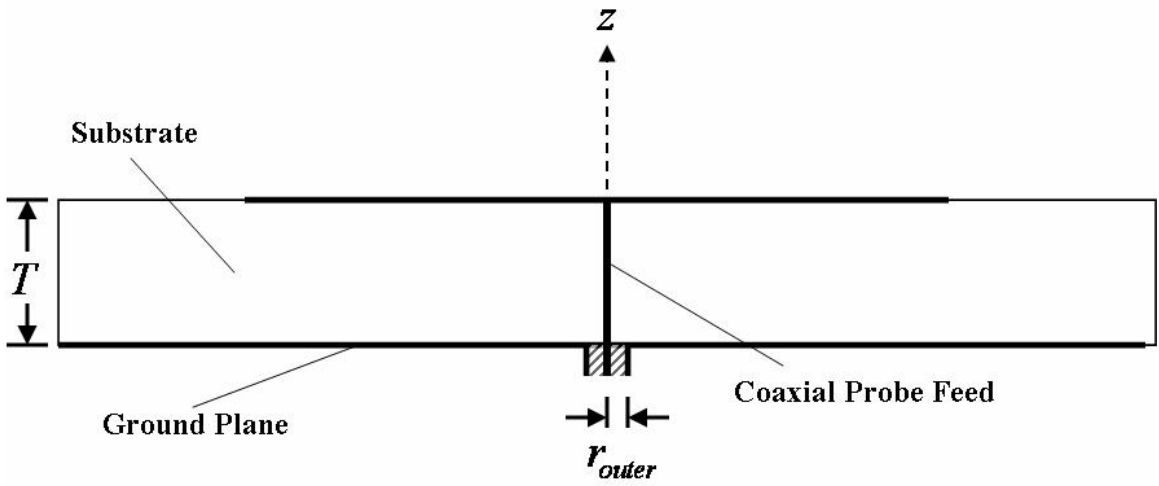
Figure 13   Topology of a Rectangular, Probe-Fed, U-Slot Microstrip Patch Antenna
on a Single-Layer, Grounded Substrate (After Ref. [18]).

D. SUBSTRATE SELECTION

Substrate selection is typically the first step in antenna design. The substrate consists of a dielectric material that affects the electrical performance of the antenna, circuits and transmission line. As a result, the substrate permittivity and thickness are critical parameters in microstrip patch antenna design. In particular, both parameters are inputs to the empirical techniques developed in [18] and [19]. It can be assumed that good selections of both parameters will yield superior performance as well as reduce the number of optimization cycles required.

The substrate must also provide mechanical support for the antenna metallization and be able to withstand the effects of the environment. The difficulty in substrate selection lies in the necessity to simultaneously satisfy the electrical and mechanical requirements. This difficulty is exacerbated in the case of aperstructures and opportunistic arrays, where the antenna element must possess the right electrical characteristics, be chemically resistant to the environment at sea but still flexible enough to conform to the ship's structure.

1. Considerations in Substrate Selection

Considerations in substrate selection, as discussed in [14], include:

1. Variations of dielectric constant and loss tangent with temperature.
2. Temperature range of homogeneity and isotropicity.
3. Variations of dimensional stability with temperature, humidity and aging.
4. Impact Resistance.
5. Resistance to chemicals.
6. Tensile and structural strength.
7. Flexibility.

Substrates can be grouped into five categories, namely, (1) ceramic, (2) semiconductor, (3) ferromagnetic, (4) synthetic and (5) composite. Table 1 lists examples of substrates from each category and some electrical and physical characteristics.

Substrate	Dielectric Constant	Loss Tangent	Dimensional Stability	Chemical Resistance	Temperature Range [degrees]	Relative Cost
Ceramic Substrates						
Alumina	9.8	0.0004	Excellent	Excellent	to +1600	Medium to high
Sapphire	9.4, 1.6	0.0001	Excellent	Excellent	-24 to +370	Very high
Semiconductor Substrates						
GaAs	13.0	0.0006	Excellent	Excellent	-55 to +260	Very High
Silicon	11.9	0.0004	Excellent	Excellent	-55 to +260	High
Ferrimagnetic Substrates						
Ferrite	9.0 to 16.0	0.001	Excellent	Excellent	-24 to +370	Medium
Synthetic Substrates						
PTFE (Teflon)	2.1	0.0004	Poor	Excellent	-27 to +260	Medium
Polypropylene	2.18	0.0003	Poor	Good	-27 to +200	Medium
Composite Material Substrates						
PTFE-glass, woven web	2.17 to 2.55	0.0009 – 0.0022	Excellent	Excellent	-27 to +260	Medium
PTFE-glass, random fiber	2.17 to 2.35	0.0009 – 0.0015	Fair	Excellent	-27 to +260	Medium to high

Table 1   Examples of Substrates and Representative Characteristics (After Ref. [14]).

2.   Theoretical Effects of Substrate Permittivity and Thickness on Performance of "Classical" Microstrip Patch Antenna

Although no accurate analytical models have been developed for the U-slot microstrip patch antenna, some of its behavior can be understood by studying the simpler "classical" microstrip patch antenna – the rectangular microstrip patch antenna. From [14], increasing the substrate thickness, T, and using substrates with lower values of dielectric constant, ε_r, can increase the bandwidth of rectangular microstrip patch antennas. This approach, however, is only useful up to $T < 0.02\lambda$. In addition, there are several disadvantages of using thick substrates with high dielectric constants, namely

1. Experimental and simulation results have shown that substrates thicker than $0.11\lambda_0$ (for $\varepsilon_r = 2.2$ and where λ_0 is the wavelength in air) make the impedance locus of the probe-fed antenna patch increasingly inductive, resulting in difficulties in impedance matching.

2. Higher order modes may develop with thick substrates, resulting in distortions of the radiation pattern.

3. Surface wave power increases with substrate thickness, resulting in poor radiation efficiency.

Next, simulation results on the effects of substrate permittivity and thickness on the performance of the U-slot microstrip patch antenna are discussed.

3. Simulation Results on the Effects of Substrate Permittivity and Thickness on Performance of U-Slot Microstrip Patch Antennas

The effects of substrate permittivity and thickness specifically on the performance of U-slot microstrip patch antennas were investigated in [20]. The scope of the results are restricted to U-slot antennas implemented on infinite, grounded dielectrics, simulated on the CAD tool IE3D and operating in the 2 GHz to 6 GHz frequency range. Nonetheless, these results provide interesting insights into the design procedures for the U-slot microstrip patch antennas intended for the aperstructure and opportunistic array concepts. The investigation procedures and results from [20] are summarized in the following paragraphs.

a. *Simulation Procedures*

Three initial U-slot antenna topologies were designed using different values of substrate permittivity – low ($\varepsilon_r = 2.2$), medium ($\varepsilon_r = 4.5$) and high ($\varepsilon_r = 9.8$). These geometries were then optimized using the parametric simulation results presented in [21] to produce broad-band impedance characteristics (2:1 *VSWR* > 20%, where *VSWR* is the Voltage Standing Wave Ratio). The substrate thicknesses were then varied and the corresponding effects on impedance bandwidth, radiation efficiency and gain were documented. For each simulation, the quantity $\dfrac{T\sqrt{\varepsilon_r}}{\lambda}$ was calculated, which describes the relative thickness of the substrate with respect to its permittivity.

b. *Effect of Substrate Thickness on Bandwidth*

Figure 14 shows that for substrates with $\varepsilon_r = 2.2$ and 4.5, the impedance bandwidths initially increase with the substrate thickness, reach a plateau at

approximately 20% to 25%, then decrease sharply. For the substrate with $\varepsilon_r = 9.8$, the impedance bandwidth has two maxima, indicating the presence of higher modes.
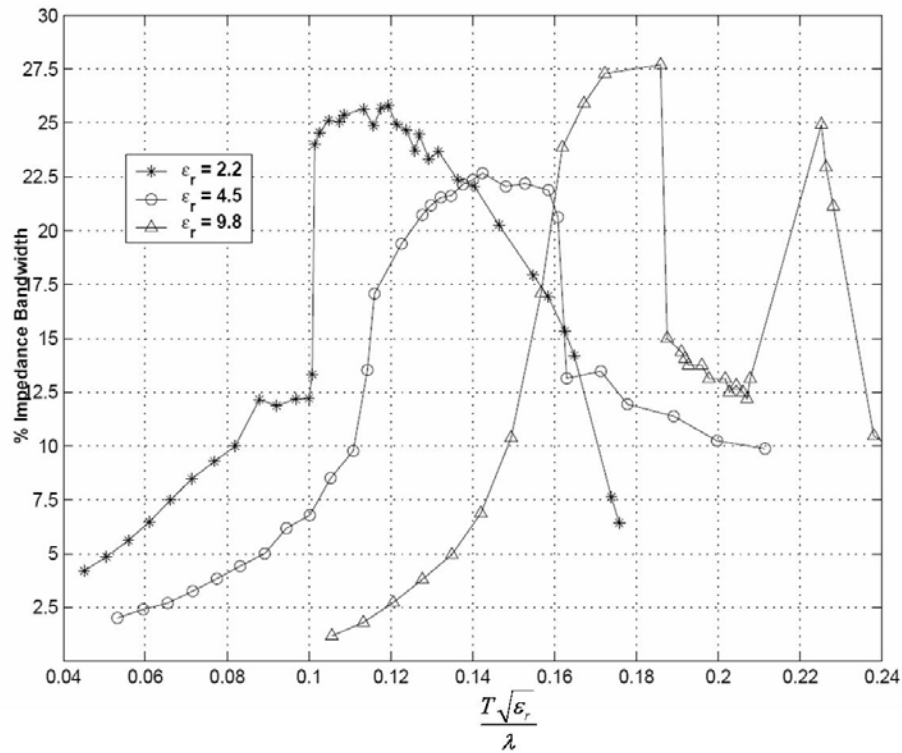
Figure 14   Effect of Substrate Thickness on Bandwidth (After Ref. [20]).

c.   *Effect of Substrate Thickness on Radiation Efficiency*

Figure 15 shows that the radiation efficiency of U-slot antennas rapidly deteriorates with the increase in substrate thickness. This phenomenon can be attributed to the excitation of higher order modes on electrically thick substrates and indicates that caution must be exercised when increasing the substrate thickness to achieve higher bandwidths.
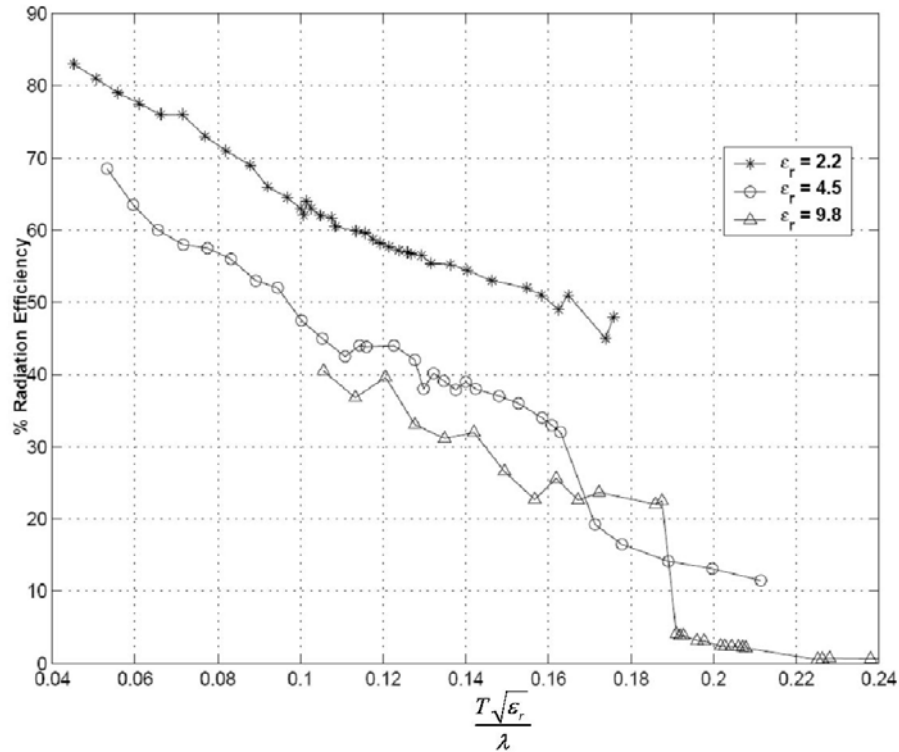
Figure 15   Effect of Substrate Thickness on Radiation Efficiency (After Ref. [20]).

d.   *Effect of Substrate Thickness on Gain*

Comparison of Figure 15 and Figure 16 shows that the gain characteristics of the U-slot antenna appear to follow its radiation efficiency. Again, this phenomenon indicates that increasing bandwidth by increasing the substrate thickness may result in a tradeoff of gain.
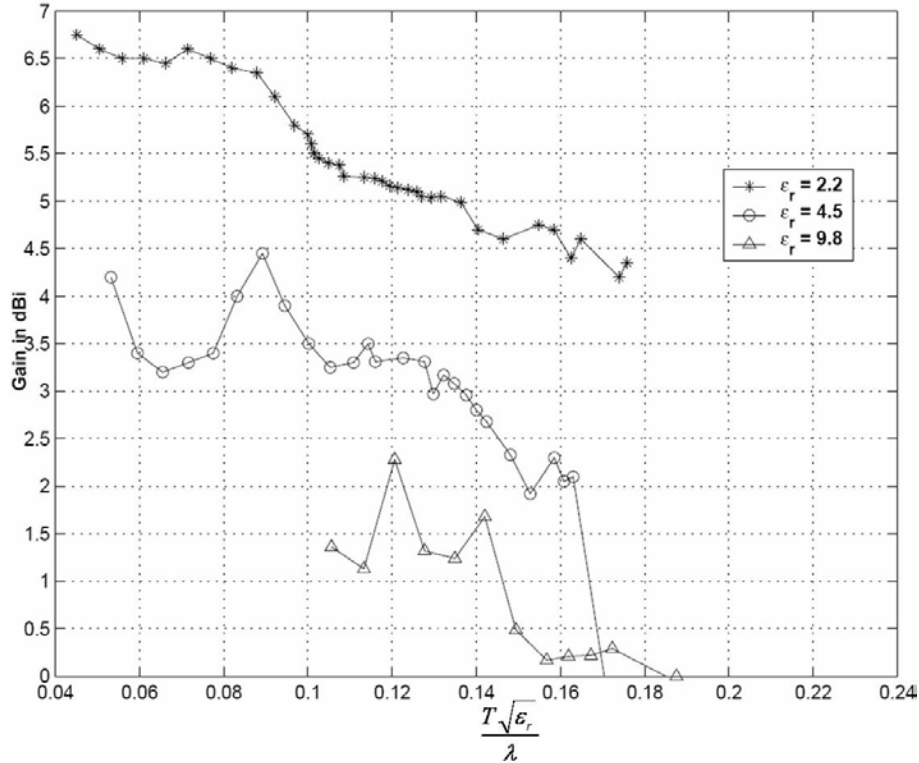
Figure 16   Effect of Substrate Thickness on Boresight Gain ($\theta = 0°, \phi = 0°$)
(After Ref. [20]).

E.   "DIMENSIONAL INVARIANCE" VS. "RESONANCE FREQUENCY" DESIGN APPROACHES

The design methodologies presented in [18] and [19] have been compared in [22] and [23]. The concepts, advantages and limitations of both methods are described in the following paragraphs. It is important to note that both methods require significant tuning to achieve broad-band behavior and it has been suggested in [23] that the number of optimization cycles needed to achieve broad-band characteristics may be used as a measure of performance.

1.   "Dimensional Invariance" Design Approach

The empirical technique in [18] is based on dimensional invariance relationships observed in the U-slot geometry and empirical design equations. The strength of this method is that it converges on the optimized design quickly – if the desired frequency lies in the range in which the design equations are reliable. The weakness of this method is that the design equations were developed for specific values of substrate permittivity and thickness. The impracticality of deriving similar equations for all possible combinations

40

of permittivity and thickness limits the usefulness of this technique. In particular, the lack of equations relevant to frequencies in the upper VHF/lower UHF bands precludes the use of this technique in this particular aperstructure and opportunistic array application.

Nonetheless, this method appears to generate initial designs that exhibit superior broad-band behavior. Hence, it may be conjectured that this technique could result in better designs if the relevant parametric equations for the upper VHF/lower UHF bands could be determined.

The advantage of the "as-is" technique, however, lies in the tuning methodology. Using the Smith chart to identify trends in the tuning procedure is a systematic method that drastically reduces the number of optimization iterations.

2. "Resonance Frequency" Design Approach

The parametric method used in [19] assumes the existence of four distinct resonant frequencies to determine the dimensions of the U-slot. It aims to balance the tradeoff between bandwidth and VSWR by keeping the VSWR at the resonant frequencies as close as possible and striving to achieve a constant VSWR over the impedance bandwidth. The result should be a centered circle on the Smith Chart plot. The strength of the method is that its design equations are based on theory, albeit a theory that was established for the rectangular, not the U-slot, microstrip patch antenna. Nonetheless, this approach results in initial designs that are close to the desired operating frequency.

There are, however, three major weaknesses in this method. First, only low permittivity substrates were studied and the applicability of the design equations to medium and high permittivity substrates was not documented. Second, the proposed design procedures may generate physically unfeasible designs. Third, the tuning technique requires significantly more iterations to achieve an optimized design.

F. PROPOSED PROCEDURES FOR INITIAL DESIGN

This thesis proposes combining the strengths of the techniques in [18] and [19] to develop a hybrid methodology – i.e. using the approach in [18] to achieve an initial

design with a center frequency close to the desired frequency. Thereafter to use the tuning technique developed in [19] to broaden the bandwidth. While both techniques have been demonstrated to work between the 2 GHz to 6 GHz frequency range, no studies have been found to indicate that these techniques would work at the upper VHF / lower UHF bands – the frequency range of interest in this thesis. The design procedures proposed in [18] are described in the following paragraphs while the tuning technique is presented in the next section.

1. Specify the center frequency and 2:1 VSWR bandwidth of the desired antenna. Approximate the center frequency as f_{res3} and the lower and upper frequency bounds of the bandwidth as f_{res2} and f_{res4} respectively.

2. Select a substrate permittivity ε_r and a substrate thickness T. There is a lower limit on T below which broad-band operation is unlikely. Therefore, the substrate thickness and permittivity should satisfy the following rule of thumb derived from the existing literature ([14], [24]) and the parametric studies

$$T \geq 0.06 \frac{\lambda_{0res3}}{\sqrt{\varepsilon_r}} \tag{3.1}$$

where λ_{0res3} = wavelength at the center frequency in air.

3. Estimate the quantity $B+2\Delta B$ as follows

$$B + 2\Delta B \approx \frac{c}{2\sqrt{\varepsilon_r} f_{res3}} \tag{3.2}$$

where c = speed of light in free space.

4. Calculate A as

$$A = 1.5(B + 2\Delta B) \tag{3.3}$$

5. Calculate the effective permittivity, ε_{eff}, and $2\Delta B$ using the following equations found in [25] and [26], respectively:

$$\varepsilon_{eff} = \frac{\varepsilon_r + 1}{2} + \frac{\varepsilon_r - 1}{2}\left(1 + \frac{12T}{A}\right)^{-1/2} \tag{3.4}$$

$$2\Delta B = 0.824T \frac{(\varepsilon_{eff} + 0.3)(\frac{A}{T} + 0.262)}{(\varepsilon_{eff} - 0.258)(\frac{A}{T} + 0.813)} \tag{3.5}$$

6. Backcalculate the value of B

$$B = \frac{c}{2\sqrt{\varepsilon_{eff}}\, f_{res3}} - 2\Delta B \qquad (3.6)$$

7. Select a starting value of slot thickness using the following rule of thumb.

$$E = F = \frac{\lambda_{0res3}}{60} \qquad (3.7)$$

8. Calculate D by solving

$$D = \frac{c}{\sqrt{\varepsilon_{eff}}\, f_{res2}} - 2(B + 2\Delta B - E) \qquad (3.8)$$

9. Select C such that

$$\frac{C}{A} \geq 0.3 \qquad (3.9)$$

$$\frac{C}{D} \geq 0.75 \qquad (3.10)$$

10. Calculate the effective permittivity and effective length extension of the pseudopatch $\varepsilon_{eff(pp)}$ of the fourth resonance with the effective patch width $D - 2F$

$$\varepsilon_{eff(pp)} = \frac{\varepsilon_r + 1}{2} + \frac{\varepsilon_r - 1}{2}\left(1 + \frac{12T}{D - 2F}\right)^{-1/2} \qquad (3.11)$$

$$2\Delta_{B-E-H} = 0.824T \frac{(\varepsilon_{eff(pp)} + 0.3)(\frac{D - 2F}{T} + 0.262)}{(\varepsilon_{eff(pp)} - 0.258)(\frac{D - 2F}{T} + 0.813)} \qquad (3.12)$$

11. Calculate H by solving

$$H \approx B - E + 2\Delta_{B-E-H} - \frac{1}{\sqrt{\varepsilon_{eff(pp)}}}\left[\frac{c}{f_{res4}} - (2C + D)\right] \qquad (3.13)$$

12. Check that the sum $C + E + H$ is less than B. If not, adjust C by changing the ratios in Step 9 and the value of H until the design is physically realizable.

G.   PROPOSED TUNING TECHNIQUE

The tuning technique in [19] requires an understanding of the relationship between the U-slot geometry and the impedance characteristics of the patch.   In

particular, the parameters that exercise significant control on the impedance loop size and location are critical to the optimization process. This section discusses the desired impedance locus on the Smith Chart, followed by the relationships between the U-slot geometry and its impedance characteristics (as investigated in [19]) and finally presents the tuning technique used in [19].

1. Characterizing Bandwidth on the Smith Chart

Figure 17 shows four generic impedance loci on a Smith Chart. Each line represents a sweep in frequency from f_{min} to f_{max}. Ideal broad-band performance is achieved when the loop of the impedance loci, such as in 1, 2 and 3, shrinks to the $VSWR = 1$ point on the Smith Chart. For practical applications, the size and location of the loop of an impedance loci is required to be such that $VSWR \leq 2$, as in locus 4. ($VSWR \leq 2$ corresponds to a return loss of 10 dB.)
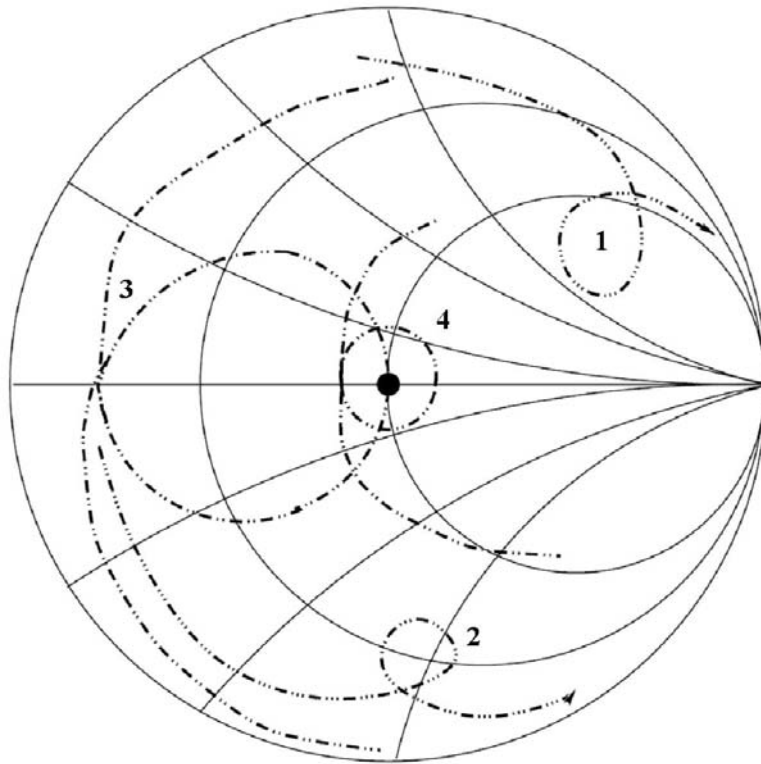
Figure 17   Generic Impedance Loci for U-Slot Microstrip Antenna. Locus 1 indicates that the design has too much inductance. Locus 2 indicates that the design has too much capacitance. Locus 3 indicates narrowband behavior. Locus 4 indicates broad-band performance (After Ref. [19]).

Figure 17 indicates that the challenge of achieving broad-band characteristics lies in examining how changes in the various dimensions shown in Figure 13 can transform loci 1, 2 and 3 to a loop similar to locus 4. Following the approach in [19], parametric studies were performed where only one parameter was changed at a time and its effect on the impedance loop noted. The results of this study provide a technique to tune the resonant frequency as well as broaden the bandwidth. While these parametric studies are not exhaustive, the results provide an insight into the antenna's behavior that can be exploited to complement the proposed initial design procedure.

2.   Investigating the Relationship between the U-Slot Geometry and the Impedance Characteristics of the Patch

In [19], five parameters were found to have significant effects on the impedance characteristics. These were (1) probe location, (2) probe radius, (3) substrate thickness, (4) slot width and (5) ratio of the distances between the U-slot and the upper edge of the patch and the lower edge of the patch (shown as $\dfrac{G}{H}$ in Figure 13). The findings in [19] are discussed in the following paragraphs.

a.   Effect of Probe Location (y_p)

Figure 18 shows the effects of varying the probe location along the y-axis on the impedance behavior of the U-slot. The results indicate that as the probe is moved in the positive direction along the y-axis, the impedance loop becomes more inductive and its size decreases.
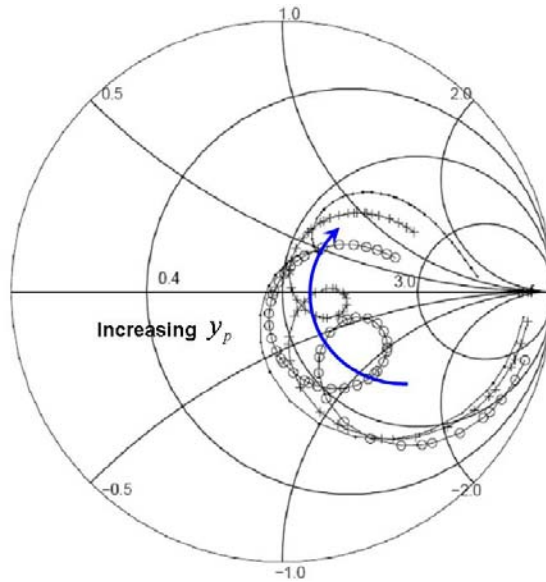
Figure 18   Effect of Probe Location on the Impedance Behavior of the U-Slot
(After Ref. [19]).

b.   *Effect of Probe Radius (r_{inner})*

Figure 19 shows the effects of varying the probe radius on the impedance behavior of the U-slot. The results indicate that variations in the probe radius do not change the size of the impedance loop, although decreasing the probe radius causes the loop to become more inductive.
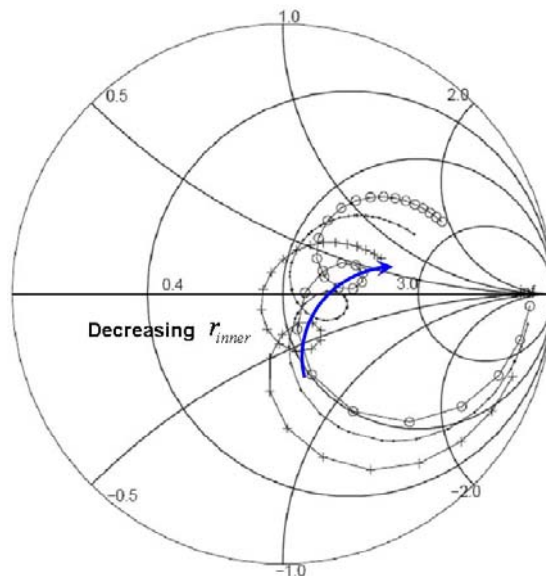
Figure 19   Effect of Probe Radius on the Impedance Behavior of the U-Slot
(After Ref. [19]).

c. ***Effect of Substrate Thickness (*T*).***

Figure 20 shows the effects of varying the substrate thickness on the impedance behavior of the U-slot. The results indicate that increasing the substrate thickness causes the impedance loop to decrease in size and also become more capacitive.
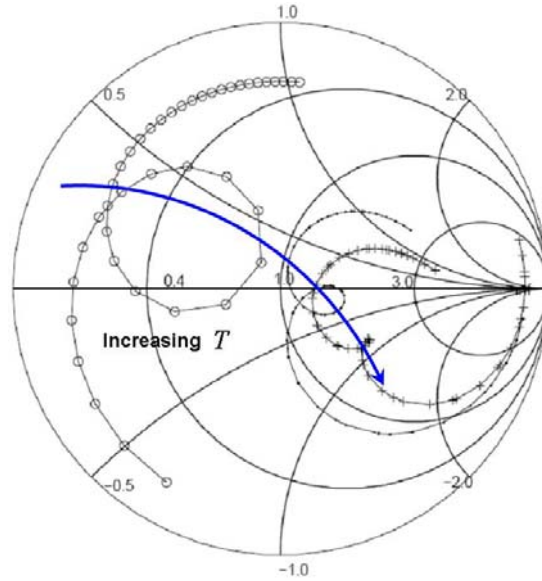
Figure 20   Effect of Substrate Thickness on the Impedance Behavior of the U-Slot (After Ref. [19]).

d. ***Effect of Slot Width (*E = F*)***

Figure 21 shows the effects of varying the slot width on the impedance behavior of the U-slot. The results indicate that as the slot width is decreased, the impedance loop becomes more inductive and its size decreases.
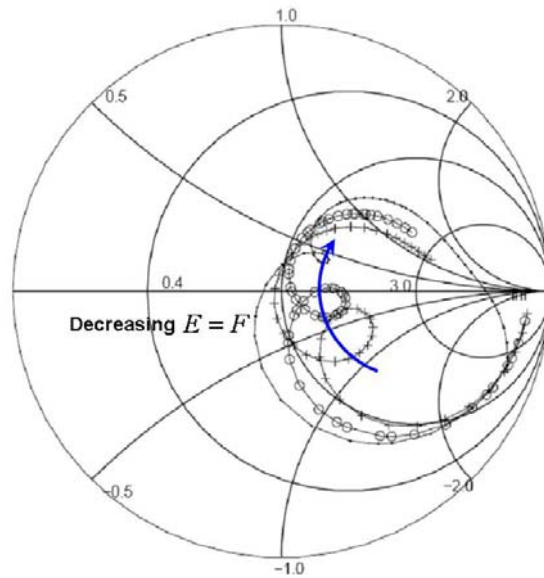
Figure 21   Effect of Slot Width on the Impedance Behavior of the U-Slot
(After Ref. [19]).

e.   **Effect of $\dfrac{G}{H}$ ratio**

Figure 22 shows the effects of varying the $\dfrac{G}{H}$ ratio on the impedance

behavior of the U-slot. The results indicate that as the $\dfrac{G}{H}$ ratio is increased, the size of

the impedance loop decreases but it becomes only slightly more inductive.
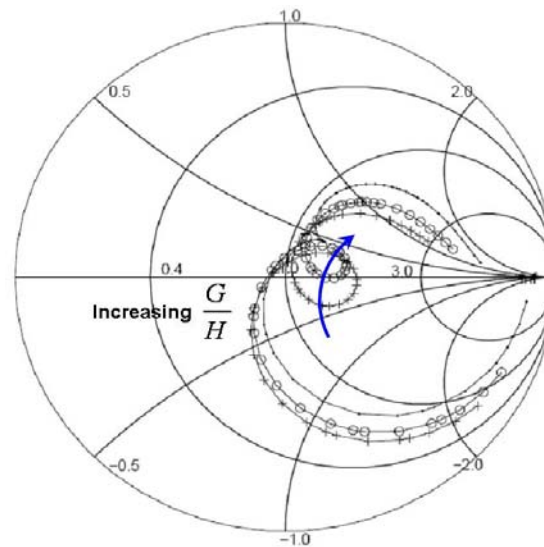
Figure 22   Effect of $\dfrac{G}{H}$ Ratio on the Impedance Behavior of the U-Slot
(After Ref. [19]).

3. Tuning Technique for Broad-band U-Slot Design

The above results suggest that the following optimization procedures, as described in [19], can be used to achieve a broad-band U-slot design.

1. Vary the substrate thickness, T, slot width, E and F, as well as probe location, y_p, such that the impedance loop encircles the center of the Smith Chart.

2. If the size of the impedance loop is undesirably large, increase the $\dfrac{G}{H}$ ratio to reduce the loop size while minimizing the effect on its location.

3. If necessary and possible, vary the probe radius, r_{inner}, as a method to refine the size and location of the impedance loop.

Again, while this technique has been demonstrated to work between the 2 GHz to 6 GHz frequency range, no studies have been found to indicate that these techniques would work at the upper VHF / lower UHF bands – the frequency range of interest in this thesis.

THIS PAGE INTENTIONALLY LEFT BLANK

IV.   SYSTEM STUDY OF APERSTRUCTURE AND OPPORTUNISTIC ARRAY CONCEPTS

A.   ANALYSIS OBJECTIVES AND PROCEDURES

In order to perform the BMD mission, it was deemed that the antenna gain and other radar system parameters must be capable of detecting targets out to 1000 km or more. The objectives of the analysis were:

1.   Verify that a detection range of at least 1000 km can be achieved.

2.   Characterize the radar performance vis-à-vis the number of active antenna elements.

A CAD model for a DD(X)-sized ship was built and various numbers of antenna elements were distributed randomly over the ship's structure. Figure 1 shows a typical array distribution.   The   MATLAB   programs   "ArrayPatternSub.m"   and "arraygainSub.m," developed by Professor David C. Jenn of the Naval Postgraduate School and Major Loke Yong of the Singapore Navy, were used to plot the beam pattern and determine the gain and average sidelobe levels numerically for various element configurations.   The   values   for   gain   were   used   in   the   MATLAB   program "ArrayPerformance.m" to characterize the performance of the radar vis-à-vis the number of active antenna elements.

B.   *AN/FPS-115 PAVE PAWS* – ACTIVE APERTURE, ELECTRONICALLY STEERED PHASE ARRAY

Equation (2.26) was used to develop a model to predict the radar performance. In order to create a realistic model, radar parameters from the AN/FPS-115 PAVE PAWS (Phased Array Warning System) were used. The AN/FPS-115 PAVE PAWS is an electronically steered phased array system developed by Raytheon and is the most similar system found in open literature [12] in terms of operational goals.

The primary mission of the PAVE PAWS radar system is to detect and track intercontinental and sea-launched ballistic missiles fired at the U.S. They have a secondary mission to perform space surveillance – to detect and track Earth-orbiting satellites as part of the U.S. Air Force Space Command. A PAVE PAWS radar employs

a dual-faced design for an azimuthal coverage of $240°$. Figure 23 shows a picture of the PAVE PAWS system at Cape Cod Air Force Station, Massachusetts. The radar parameters of the AN/FPS-115 PAVE PAWS system, as given in [12], are shown in Table 2. These parameters will be assumed in the subsequent radar system analysis.

Figure 23   PAVE PAWS UHF, Solid-state, Dual-faced Radar System in Cape Cod Air Force Station, Massachusetts (From Ref. [27]).

Operating Frequency	420 to 450 MHz
Peak Power	600 kW
Average Power	150 kW
Duty Cycle	0.25
Pulse Width	16 ms
Predicted Range	3000 nm (10 m^2 target)

Table 2   Radar Parameters for AN/FPS-115 PAVE PAWS Radar System (After Ref. [12]).

C.   BROADSIDE SIMULATION RESULTS ($\phi_S = 90°$)

First, a broadside scan condition is simulated. In the simulation, it was assumed that the element factor was hemispherical and that the element gain was a maximum in the direction normal to the facet surface on which it resides. The MATLAB simulations numerically determined the azimuth gain and sidelobe levels, among other quantities, for broadside scan ($\phi_S = 90°$) at an elevation of 10 degrees ($\theta_S = 80°$). Figure 24 shows a plot of the relative power pattern versus azimuth angle. Figure 25 shows the radiation

pattern of the entire aperstructure in a three-dimensional polar format. At this scan angle, simulation results consistently indicated that approximately 65% of the total antenna elements were active. Hence, it appears that the number of active antenna elements can be predicted given the total number of antenna elements.

Figure 24   Plot of Relative Power Pattern Against Azimuth Angle (Total Number of Elements = 1200, $\phi_S = 90°$, $\theta_S = 80°$).

Figure 25   Radiation Pattern of Aperstructure (Total Number of Elements = 1200, $\phi_S = 90°$, $\theta_S = 80°$).

1.   Average Sidelobe Level – Theoretical vs. Numerical

The relationship between the expected sidelobe level and number of active antenna elements was predicted in Equation (2.11). Figure 26 shows the results of the simulation as compared to the predicted relationship. The simulation results exhibit oscillatory behavior that can be attributed to the random distribution and orientation of antenna elements. From Figure 26, it is observed that the simulation results are consistent with the theoretical predictions.

Figure 26   Relationship Between Relative Sidelobe Level [dB] and Number of Active Antenna Elements ($\phi_S = 90°$ and $\theta_S = 80°$).

2.   Main Lobe Gain – Theoretical vs. Numerical

The relationship between the expected gain of the main lobe and the number of active antenna elements was predicted in Equation (2.18). Figure 27 shows the results of the simulation as compared to the theoretically predicted relationship. Again, the simulation results exhibit oscillatory behavior that can be attributed to the random distribution of antenna elements. From Figure 27, it is observed that the simulation results are consistent with the theoretical predictions.

Figure 27   Relationship Between Gain [dB] and Number of Active Antenna
Elements ($\phi_S = 90°$ and $\theta_S = 80°$).

3.   Radar Theoretical Maximum Range vs. Total Number of Antenna Elements

The radar's theoretical maximum range was given in Equation (2.26). Using the values of gain determined for various numbers of elements, the relationship between the theoretical maximum range and the total number of antenna elements can be determined. Figure 28 shows this relationship for $N = 400$, 800 and 1200. Assuming that each element delivers an average power of approximately 500 W, only 400 elements are required to achieve a theoretical maximum range of 1000 km. If 800 elements are available, a theoretical maximum range of approximately 1600 km is possible. If 1200 elements are available, a theoretical maximum range beyond 2000 km is possible.

Figure 28   Relationship Between Radar Theoretical Maximum Range and Total Number of Antenna Elements ($\phi_S = 90°$ and $\theta_S = 80°$).

D.   ENDFIRE SIMULATION RESULTS ($\phi_S = 180°$)

Figure 24 shows a plot of the relative power pattern versus azimuth angle when the beam is scanned in the forward direction. This is an endfire condition for the array. Figure 25 shows the radiation pattern of the entire aperstructure. At this scan angle, simulation results consistently indicated that approximately 95% of the total antenna elements were active. That is, 95% of the elements have at least a part of their FOV toward the bow of the ship.
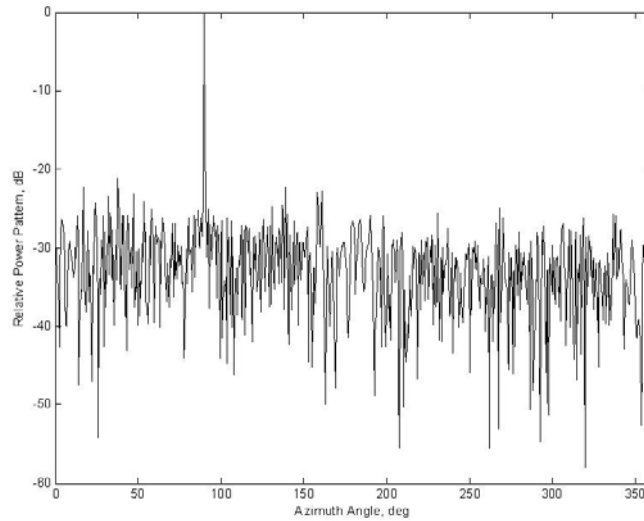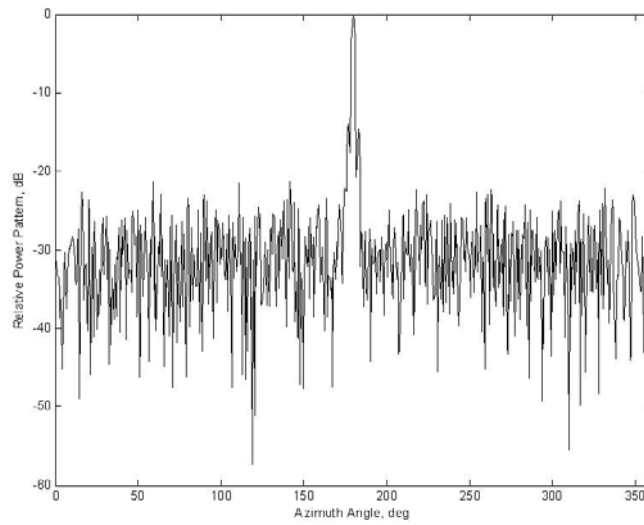
Figure 29   Plot of Relative Power Pattern Against Azimuth Angle (Total
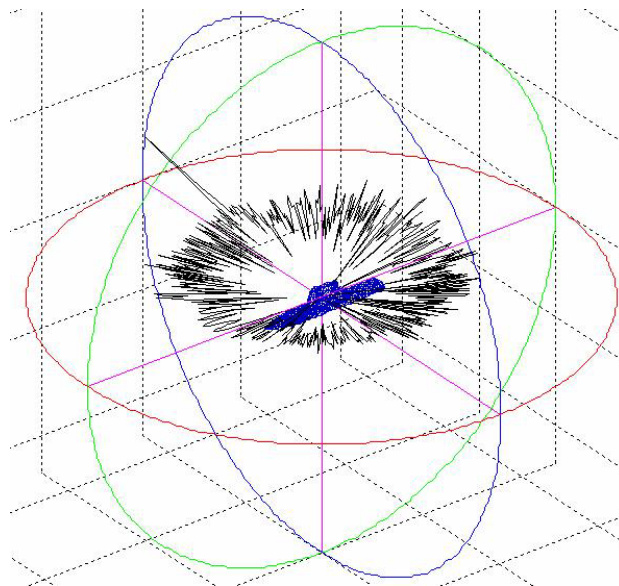Number of Elements = 1200, $\phi_S = 180°$ and $\theta_S = 80°$).
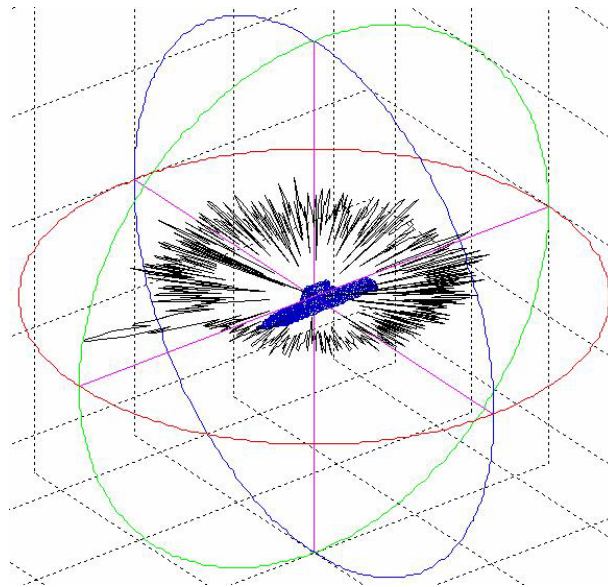
Figure 30   Radiation Pattern of Aperstructure (Total Number of Elements = 1200,
$\phi_S = 180°$ and $\theta_S = 80°$).

1.   Average Sidelobe Level – Theoretical vs. Numerical

Figure 31 shows the results of the simulation as compared to the predicted
relationship. The simulation results exhibit oscillatory behavior that can be attributed to

the random distribution of antenna elements. From Figure 31, it is observed that the simulation results are consistent with the theoretical predictions.
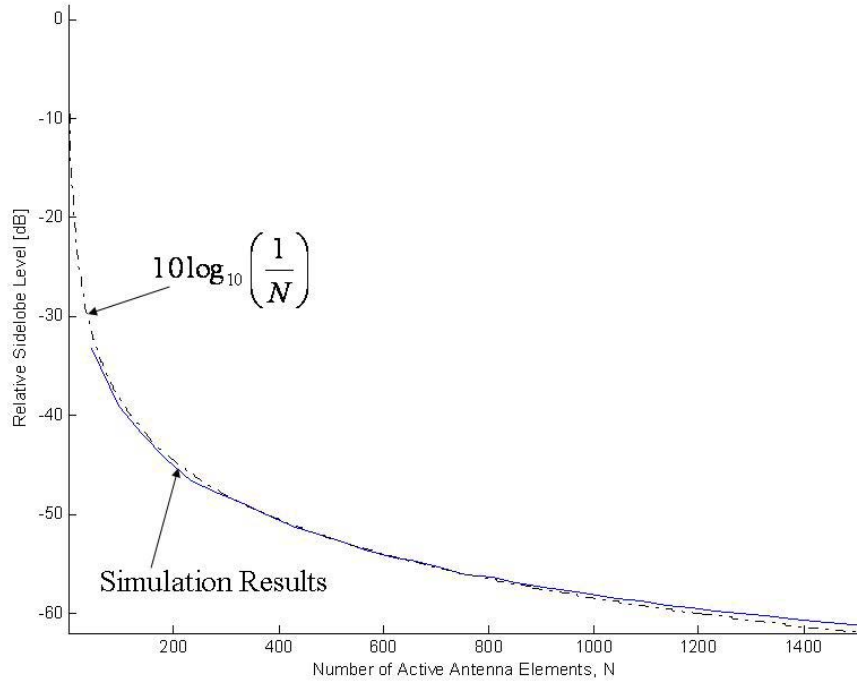
Figure 31   Relationship Between Relative Sidelobe Level [dB] and Number of Active Antenna Elements ($\phi_S = 180°$ and $\theta_S = 80°$).

2.   Main Lobe Gain – Theoretical vs. Numerical

Figure 32 shows the results of the simulation as compared to the theoretically predicted relationship. Again, the simulation results exhibit oscillatory behavior that can be attributed to the random distribution of antenna elements. From Figure 32, it is observed that the simulation results are consistent with the theoretical predictions.
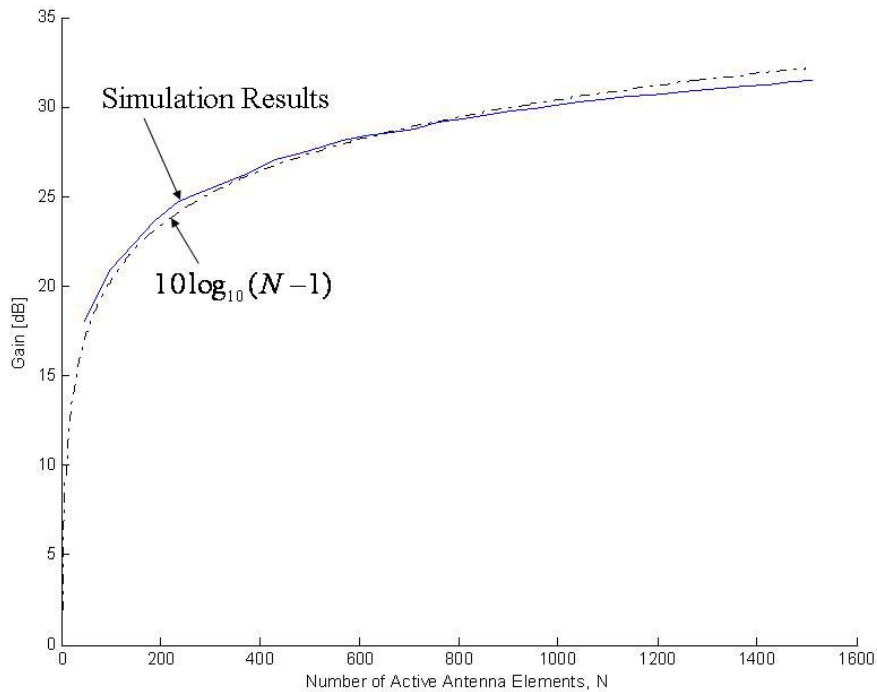
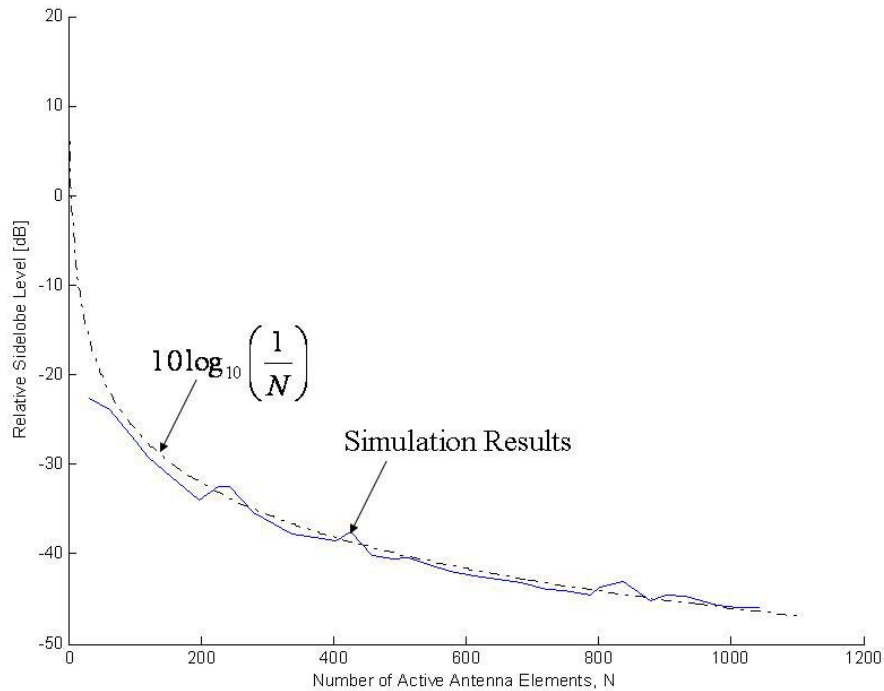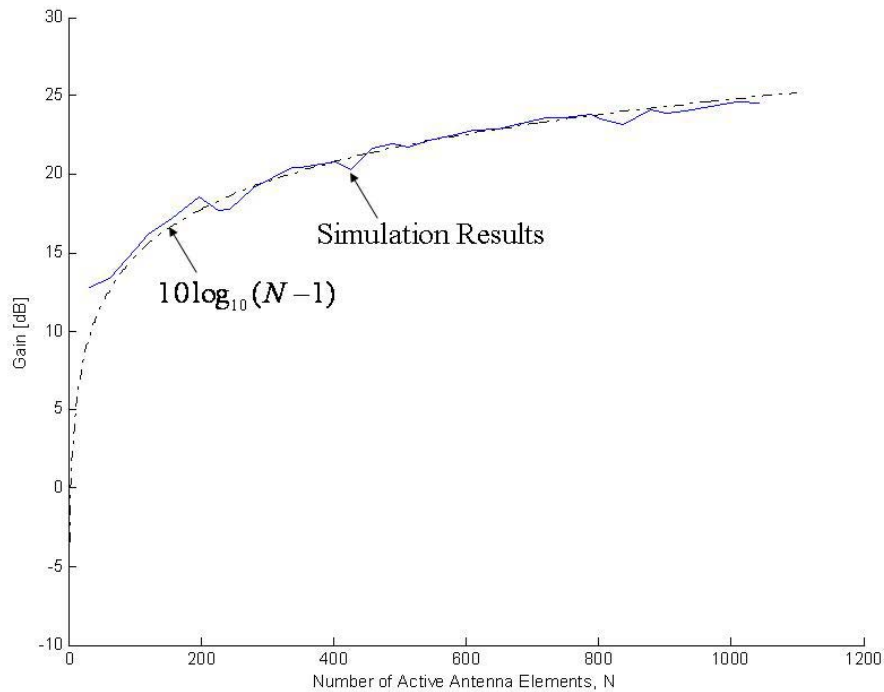Figure 32   Relationship Between Gain [dB] and Number of Active Antenna Elements ($\phi_S = 180°$ and $\theta_S = 80°$).

3. Radar Theoretical Maximum Range vs. Total Number of Antenna Elements

Figure 33 shows the relationship between the theoretical maximum range and total number antenna elements for $N = 400$, 800 and 1200. Observe that each element is only required to deliver an average power of approximately 50 W to achieve a theoretical maximum range beyond 1000 km. This result, however, is likely to be overly-optimistic because of the hemispherical element factor assumption. The elements' FOV will probably be more narrow than a hemisphere (which is a constant gain versus angle) and hence fewer elements will contribute to the gain at endfire.
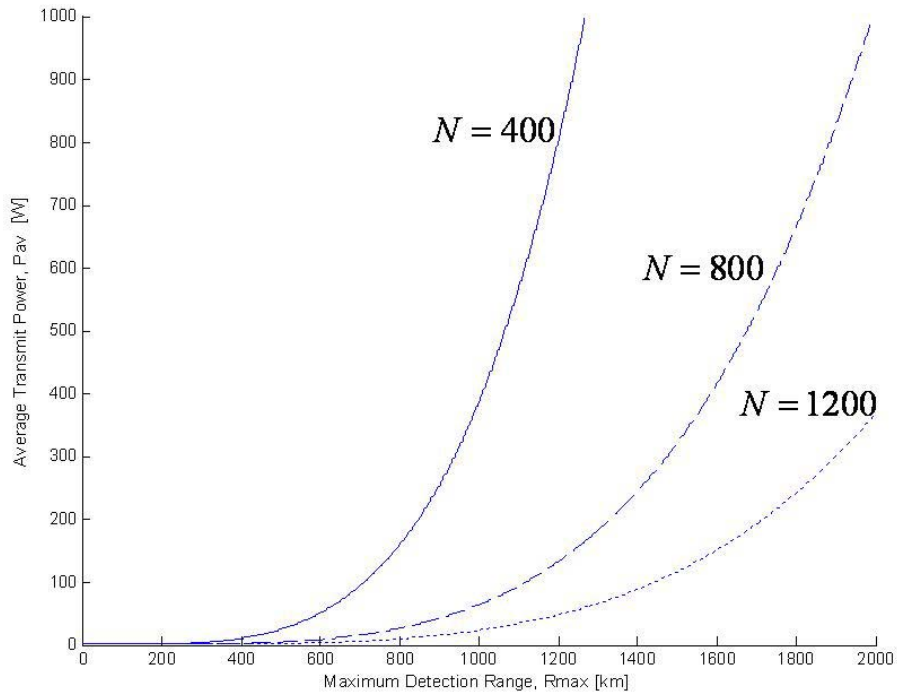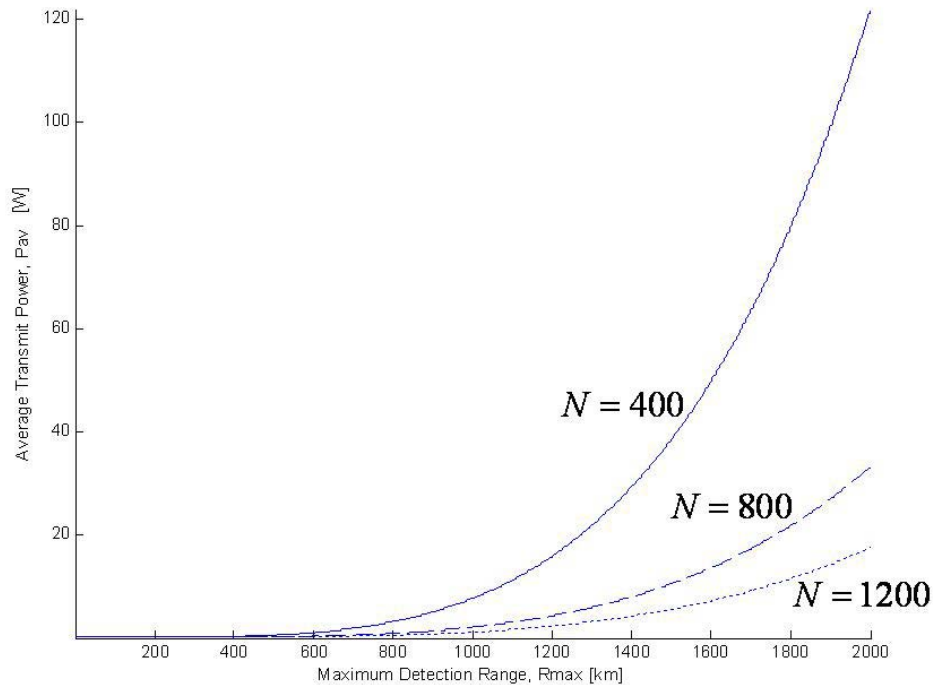
Figure 33   Relationship Between Radar Theoretical Maximum Range and Total
Number of Antenna Elements ($\phi_S = 180°$ and $\theta_S = 80°$).

E.   ANALYSIS OF RESULTS

The broadside and endfire simulation results are best analyzed separately because of the limitations of the simulation programs.

1.   Broadside Simulation Results

Figure 26 and Figure 27 show that it is possible to predict the relative sidelobe level and main lobe gain given the number of active antenna elements. In addition, since the ratio of active antenna elements to total antenna elements is approximately constant for a given scan angle, the radar performance for a given angle can be predicted with the total number of antenna elements. Figure 28 verifies that a detection range of at least 1000 km can be achieved with as little as a total of 400 antenna elements, assuming each element radiates 500 W. This power level is not unreasonable given the existence of BMD radars such as the AN/FPS-115 PAVE PAWS.

2.   Endfire Simulation Results

Figure 31 and Figure 32 show that the simulation results for the relative sidelobe level and main lobe gain agree closely with the theoretical predictions. While the ratio of

active antenna elements to total antenna elements was found to be approximately constant for the given scan angle, it appeared unusually high (95%). Figure 34 shows the relationship between the number of active antenna elements and observation angle, for a total of 1200 antenna elements. Figure 34 is representative of the relationship between the number of active antenna elements and observation angle for other values of N.

There appears to be unusually high numbers of active antenna elements at observation angles $\phi = 0°$ and $\phi = 180°$. This appears to be a result of a limitation in the MATLAB programs "ArrayPatternSub.m" and "arraygainSub.m". In these programs, the radiation patterns of individual antenna elements were assumed to be perfectly hemispherical. As a result, an element was considered active as long as the dot product between its normal and the observation angle was positive. This occurs most at observation angles of $\phi = 0°$ and $\phi = 180°$. Even though most elements are pointed in the general direction of broadside, they still have the edges of their FOV in the endfire direction and these contribute to array gain. There is also less obstruction by the ship's structure to the observation point. In reality, however, the radiation pattern of an antenna element is unlikely to be hemispherical. Hence, the simulation results for scan angles $\phi_S = 0°$ and $\phi_S = 180°$ are overly-optimistic. Nonetheless, it indicates that 360° operation is possible, if desired.
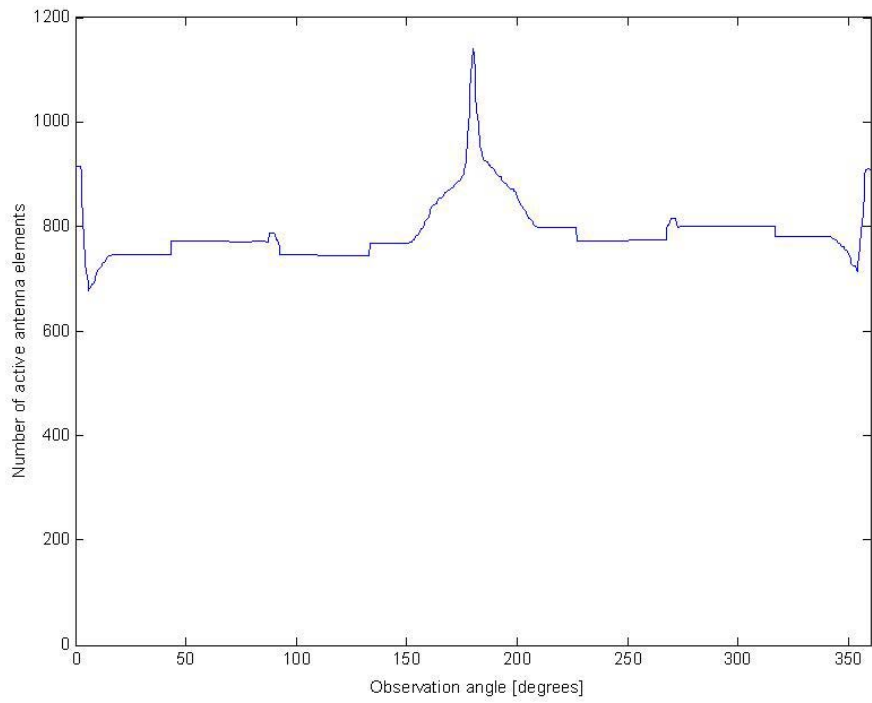
Figure 34   Relationship between Number of Active Antenna Elements and
Observation Angle for $N = 1200$.

V. DESIGN OF LOW-PROFILE, BROAD-BAND, PROBE-FED, U-SLOT MICROSTRIP PATCH ANTENNAS FOR APERSTRUCTURES AND OPPORTUNISTIC ARRAYS

A. DESIGN OBJECTIVES AND PROCEDURES

The aperstructure concept requires the antenna elements to be integrated into the structure of the ship. The aperstructure should also be able to perform both radar and communication functions – resulting in a requirement for broad-band characteristics. In addition, since the operating frequency has not yet been decided upon, it is imperative to develop a systematic set of design procedures for patch antennas operating in the upper VHF / lower UHF frequency band. Hence, the primary objectives of the design efforts were:

1. Design a low-profile patch antenna with broad-band characteristics necessary for radar and communication functions.

2. Develop a set of design procedures that result in a good "first-pass" design with prescribed characteristics that require minimal tuning.

The simulation tool CST Microwave Studio was first validated against published experimental and computed data for the U-slot geometry. Next, the type of substrate and coaxial feed were selected. The effects of variations in the U-slot dimensions on the impedance characteristics were then investigated using CST Microwave Studio. Thereafter, an initial design was created and optimized.

B. VALIDATION OF CST MICROWAVE STUDIO RESULTS

Leveraging on a simulation tool such as CST Microwave Studio to design the microstrip patch antenna dramatically enhances the efficiency of the design process – both in terms of time and costs. However, this results in the success of the design hinging entirely on the accuracy of the CAD tool. Subsequently, it is critical that CST Microwave Studio is validated against appropriate test cases that are closest to the topology being studied.

Experimentally measured and numerically computed data for a U-slot design was found in [28]. The center frequency of the chosen design (referred to as "Antenna B" in [28]), however, was 3.56 GHz – outside the upper VHF / lower UHF frequency range.

Nonetheless, the data from [28] would be sufficient to validate the accuracy of CST Microwave Studio because of the similar topology [29].

1.   Topology of Test Case.

The dimensions of Antenna B, as obtained from [19] and [28], are presented in Table 3.

ε_r	A [mm]	B [mm]	C [mm]	D [mm]	E [mm]	F [mm]	G [mm]	H [mm]	T [mm]	y_p [mm]	r_{inner} [mm]
2.33	36	26	16	14	2	2	4	4	6.4	0	0.635

Table 3   Dimensions of U-Slot Microstrip Patch Antenna Used to Validate CST Microwave Studio (After Ref. [28]).

2.   Validation Results

The results obtained using CST Microwave Studio will be compared with both experimentally measured as well as numerically computed results from [28]. Note that the numerically computed results in [28] were obtained using a frequency domain method known as the finite-difference time-domain (FDTD) method. CST Microwave Studio uses a different frequency domain method known as the finite integration (FI) method. Subsequently, small differences in results should be expected. The center frequency, f_{center}, upper cut-off frequency, f_{upper}, lower cut-off frequency, f_{lower}, absolute bandwidth, BW, and percentage bandwidth, $\%BW$, as obtained from [28] and CST Microwave Studio are shown in Table 4. The impedance characteristics as obtained from [28] and CST Microwave Studio are shown in the Smith Charts in Figure 35.

	f_{lower} [GHz]	f_{center} [GHz]	f_{upper} [GHz]	BW [GHz]	$\%BW$
Results from [28]					
Computed	2.87	3.28	3.69	0.82	25.0
Measured	2.76	3.16	3.56	0.80	25.3
Results from CST Microwave Studio					
Computed	2.73	3.08	3.43	0.70	22.7

Table 4   Operating Frequencies and Bandwidth Results (From Ref. [28] and CST Microwave Studio.

(a)	(b)
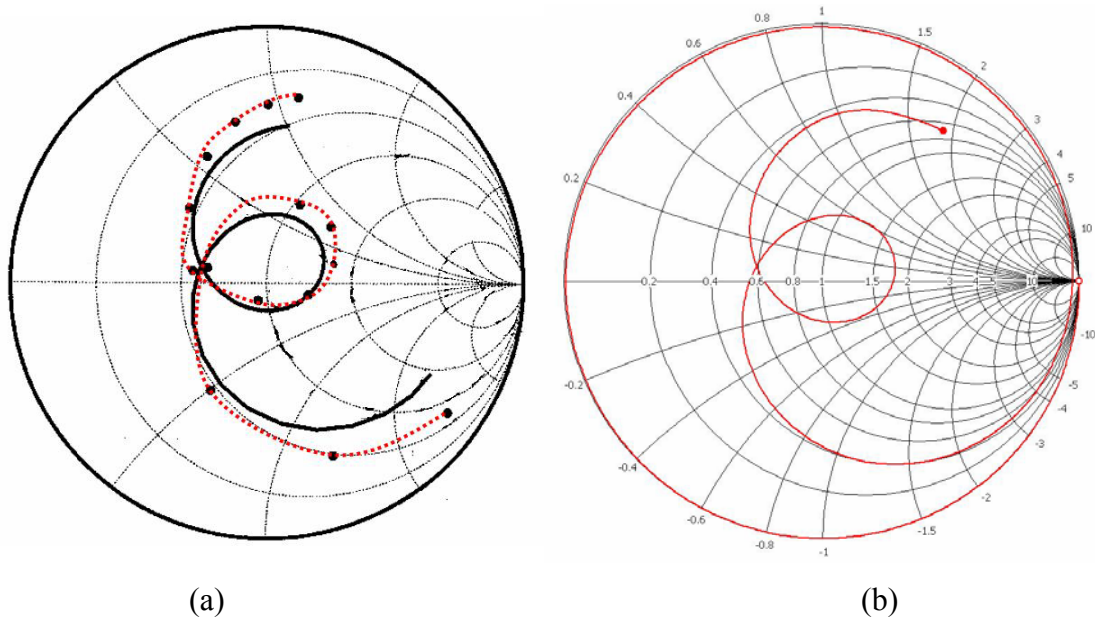
Figure 35　　　　Impedance Characteristics. (a) Impedance Loci from [28] − Solid Line Indicates Computed Results and Red Dotted Line Indicates Measured Results (After Ref. [28]) (b) Impedance Locus for Test Case Simulated Using CST Microwave Studio.

Table 4 and Figure 35 show that there is good agreement between the results from CST Microwave Studio and the published results from [28].

C.　　SUBSTRATE SELECTION

From Table 1, it was deduced that a composite material substrate, woven web PTFE (Teflon)-glass, would be desirable for the aperstructure application. It provides excellent dimensional stability and chemical resistance necessary for a sea-based application. It also allows operation in a wide temperature range ($-26°$ to $+260°$) and is relatively cost-effective. Present ceramic substrates, while possessing superior operating temperature ranges, are brittle. Hence, they are unsuitable for integrating into the hull of a ship as there is a risk that the ceramic substrate will break when the ship structure flexes.

The relative permittivity, ε_r, of the woven web PTFE-glass substrate, as listed in Table 1, is between 2.17 to 2.55. A value of $\varepsilon_r = 2.33$ was selected, similar to the test cases in [28].

D.   CHOICE OF COAXIAL FEED

A semi-rigid coaxial cable was chosen for the feed. The primary reason for this choice was that semi-rigid coaxial feeds have high power handling efficiencies. Table 5 shows the specifications of a semi-rigid coaxial feed produced by Micro-Coax. Note that at an operating frequency of 500 MHz, the product is specified to handle 600 W with an insertion loss of 0.26 dB/m. Figure 36 shows an illustration of the UT-141-HA-M17 Semi-Rigid Coaxial Cable Produced by Micro-Coax.

Mechanical Characteristics			
Outer Conductor Diameter	3.581 +/- 0.0254 [mm]		
Dielectric Diameter	2.985 [mm]		
Center Conductor Diameter	0.919 +/- 0.0178 [mm]		
Weight	5.12 [kg/100m]		
Electrical Characteristics			
Impedance	50 +/- 1.0 [Ω]		
Frequency Range	DC to 20 [GHz]		
Capacitance	29.9 [pF/m]		
	Frequency [GHz]	Insertion Loss [dB/m]	Power [W]
Typical Insertion Loss	0.5	0.26	600
	1.0	0.39	450
	5.0	0.95	250
Materials			
Outer Conductor	Copper		
Dielectric	Teflon (PTFE)		
Center Conductor	Silver Plated Copper Weld (SPCW)		

Table 5   Specifications of Semi-Rigid Coaxial Feed (After Ref. [31]).

Figure 36   UT-141-HA-M17 Semi-Rigid Coaxial Cable Produced by Micro-Coax
(After Ref. [31]).

E.   PARAMETRIC MODELING STUDIES USING CST MICROWAVE STUDIO

The relationship between the U-slot geometry and the impedance characteristics of the patch was investigated using CST Microwave Studio. Similar to the parametric modeling studies in [19], the parameters studied were (1) probe location, (2) substrate thickness, (3) slot width and (4) ratio of the distances between the U-slot and the upper edge of the patch and the lower edge of the patch (shown as $\dfrac{G}{H}$ in Figure 13). However, the effect of varying the probe radius was intentionally omitted. This was because variations in the probe radius produced the least tuning effect. Moreover, its only advantage as a "fine-tuning" mechanism is nullified as commercial probe feeds are available only in standard sizes – not continuous sizes that are useful for "fine-tuning" the design. The results of the parametric modeling studies using CST Microwave Studio are discussed in the following paragraphs. Note that the Smith Charts produced by CST Microwave Studio have several impedance loops. The loop closest to the center of the Smith Chart is the loop of interest. The other loops indicate minor modes of resonance that were created because of the requirement in CST Microwave Studio to simulate beyond the frequency range of interest [30].

67

1. Effect of Probe Location (y_p)

Figure 37 shows the effects of varying the probe location along the y-axis on the impedance behavior of the U-slot. The results indicate that as the probe is moved in the negative y-direction, the impedance loop becomes more capacitive and its size increases slightly. This is similar to the findings in [19].

| | | |
| (a) | (b) | (c) |
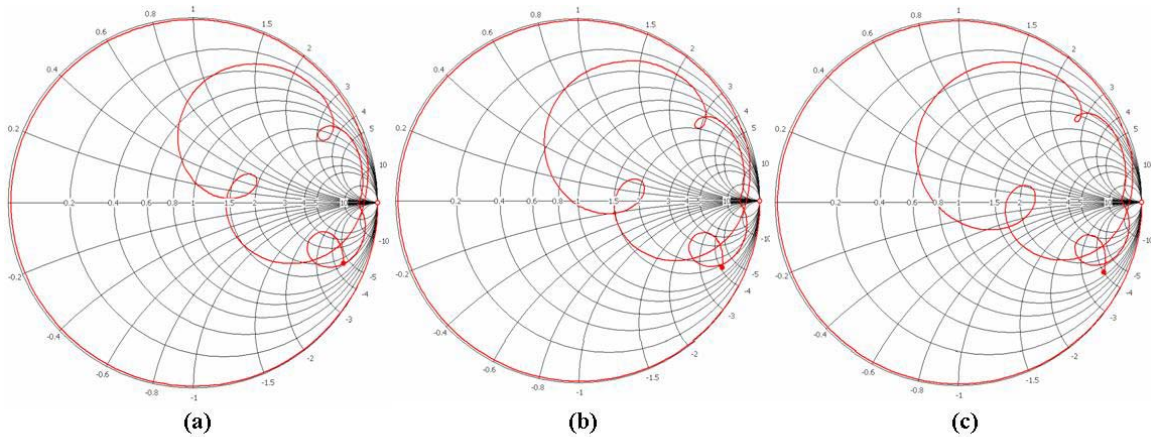
Figure 37   Effect of Probe Location on the Impedance Behavior of the U-Slot.
(a) $y_p = 0$ mm, (b) $y_p = -5$ mm, (c) $y_p = -10$ mm.

2. Effect of Substrate Thickness (T)

Figure 38 shows the effects of varying the substrate thickness on the impedance behavior of the U-Slot. The results indicate that increasing the substrate thickness causes the impedance loop to decrease in size and also become more capacitive. This is similar to the findings in [19]. However, Figure 38 also shows that there is a limit beyond which increasing the substrate thickness results in loss of the resonance condition.
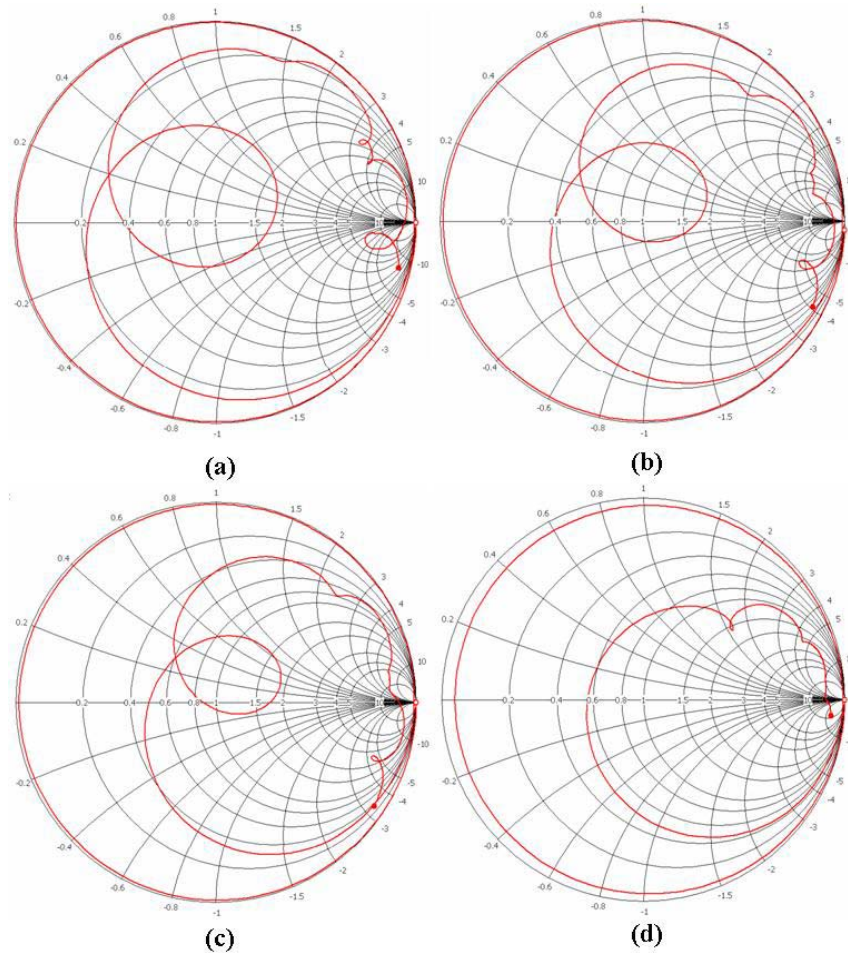
Figure 38   Effect of Substrate Thickness on the Impedance Behavior of the U-Slot
                 (a) $T = 40$ mm, (b) $T = 50$ mm, (c) $T = 55$ mm, (d) $T = 60$ mm.

3.   Effect of Slot Width ($E = F$)

Figure 39 shows the effects of varying the slot width on the impedance behavior of the U-slot. The results indicate that as the slot width is increased, the impedance loop becomes more capacitive and its size increases slightly. This is consistent with the results from [19].

(a)   (b)   (c)
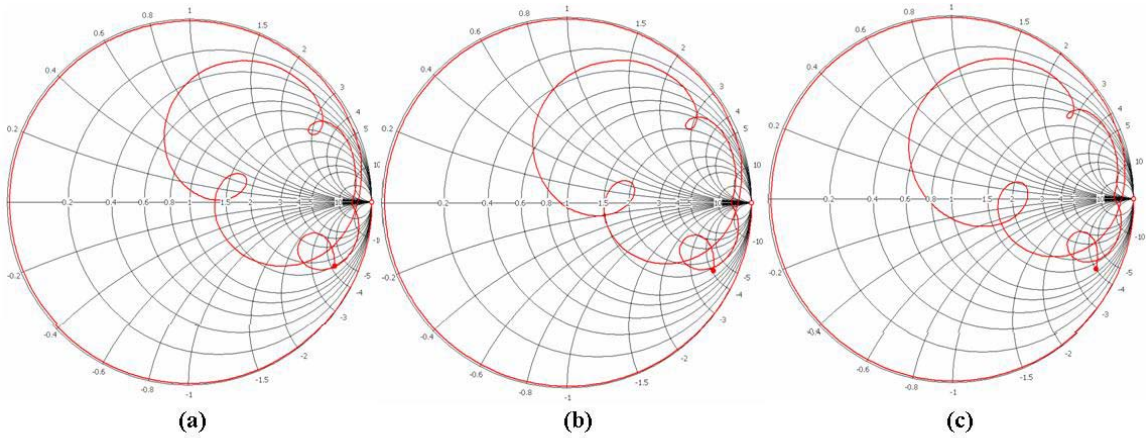
Figure 39   Effect of Slot Width on the Impedance Behavior of the U-Slot
(a) $E = F = 14$ mm, (b) $E = F = 15$ mm, (c) $E = F = 16$ mm,

4.   Effect of $\dfrac{G}{H}$ Ratio

Figure 40 shows the effects of varying the $\dfrac{G}{H}$ ratio on the impedance behavior of

the U-slot.   The results indicate that as the $\dfrac{G}{H}$ ratio is decreased, the size of the

impedance loop increases and becomes only slightly more capacitive.   This is consistent
with the results from [19].

(a)   (b)   (c)
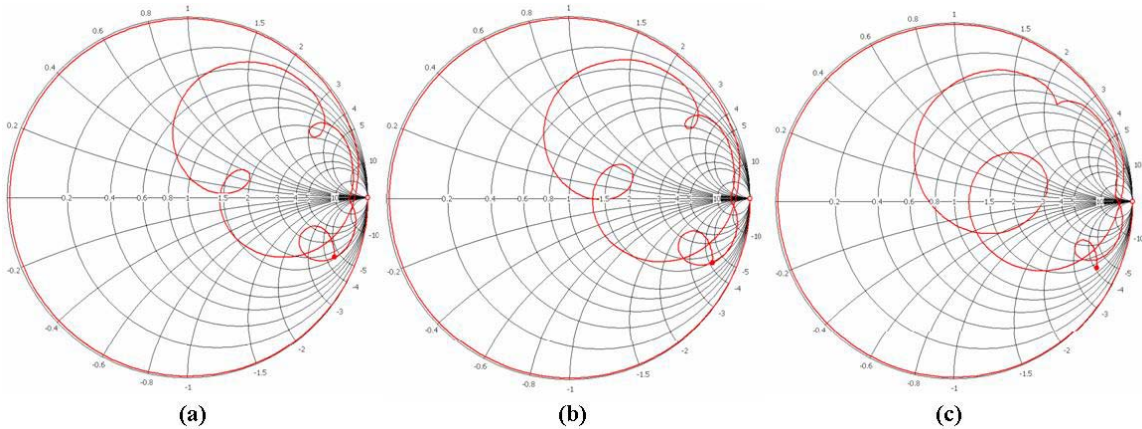
Figure 40   Effect of $\dfrac{G}{H}$ Ratio on the Impedance Behavior of the U-Slot

(a) $\dfrac{G}{H}=7$, (b) $\dfrac{G}{H}=5$, (c) $\dfrac{G}{H}=2$.

F.   BROAD-BANDING – THE SMITH CHART APPROACH

The above results suggest that the tuning technique in [19] can be used in the upper VHF / lower UHF frequency range too.   Hence, the following optimization procedures can be used to achieve a broad-band U-slot design.

1.   Vary the substrate thickness, T, slot width, E and F, as well as probe location, y_p, such that the impedance loop encircles the center of the Smith Chart.

2.   If the size of the impedance loop is undesirably large, increase the $\dfrac{G}{H}$ ratio to reduce the loop size while minimizing the effect on its location.

These procedures will be used to tune the initial design in the next section.

G.   INITIAL DESIGN

The proposed design procedures described in Chapter III Section F were used to create an initial design with a center frequency of 300 MHz.   The dimensions of the initial design are shown in Table 6.   Figure 41 shows the resulting Smith Chart.   From Figure 41, it can be deduced that the design would likely exhibit narrow-band behavior. This is confirmed in Figure 42, which shows the return loss for the initial design.   From Figure 42, it is observed that the initial design has a center frequency of 346 MHz and a bandwidth of 24 MHz (7%).   Figure 43 shows the far-field pattern for $\phi = 0°$.   Figure 44 shows the far-field pattern for $\phi = 90°$.   Figure 43 and Figure 44 show that the initial design produces in a good radiation pattern.

ε_r	A [mm]	B [mm]	C [mm]	D [mm]	E [mm]	F [mm]	G [mm]	H [mm]	T [mm]	y_p [mm]	r_{inner} [mm]
2.33	421.1	253.6	170	115	14.3	14.3	13.2	56.1	40	0	0.46

Table 6   Initial Design of 300 MHz U-Slot Microstrip Patch Antenna.

Figure 41   Impedance Locus for Initial Design of 300 MHz U-Slot Microstrip Patch
Antenna Indicating Narrow-band Behavior.

Figure 42   Return Loss for Initial Design of 300 MHz U-Slot Microstrip Patch
Antenna Indicating a Center Frequency of 346 MHz and Bandwidth of 24 MHz

(7%).

Figure 43   Far-field Radiation Pattern of Initial Design for $\phi = 0°$ at 300 MHz.

Figure 44   Far-field Radiation Pattern of Initial Design for $\phi = 90°$ at 300 MHz.

H. OPTIMIZED DESIGN

The initial design was optimized using the outlined design procedures. Table 7 shows the dimensions of the optimized design. Figure 45 shows the resulting Smith Chart. From Figure 45, it can be deduced that the design would likely exhibit broad-band behavior. This is confirmed in Figure 46, which shows the return loss for the optimized design. From Figure 46, it is observed that the optimized design has a center frequency of 316 MHz and a bandwidth of 63 MHz (20%). Figure 47 shows the far-field pattern for $\phi = 0°$. Figure 48 shows the far-field pattern for $\phi = 90°$. Figure 47 and Figure 48 show that the optimized design produces in a good radiation pattern.

ε_r	A [mm]	B [mm]	C [mm]	D [mm]	E [mm]	F [mm]	G [mm]	H [mm]	T [mm]	y_p [mm]	r_{inner} [mm]
2.33	421.1	253.6	170	115	14.3	14.3	55.44	13.86	55	-30	0.46

Table 7   Optimized Design of 300 MHz U-Slot Microstrip Patch Antenna.
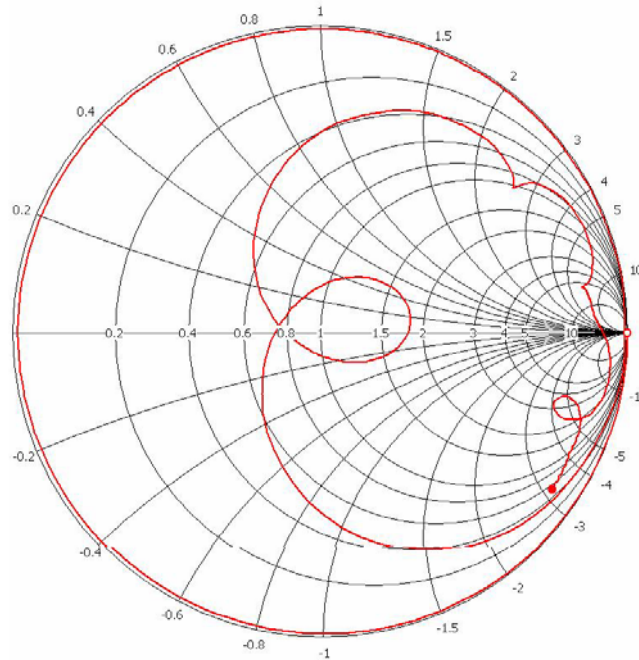
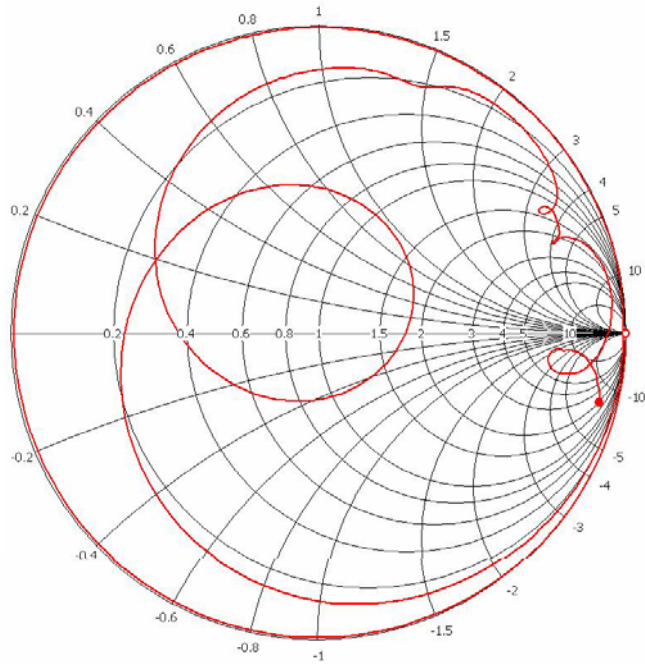Figure 45   Impedance Locus for Optimized Design of 300 MHz U-Slot Microstrip Patch Antenna Indicating Broad-band Behavior.
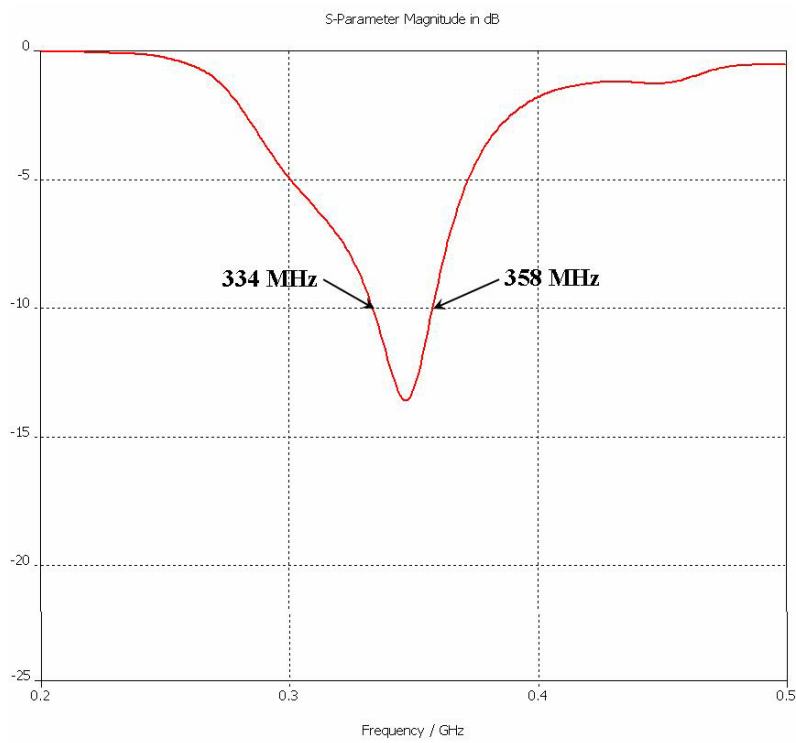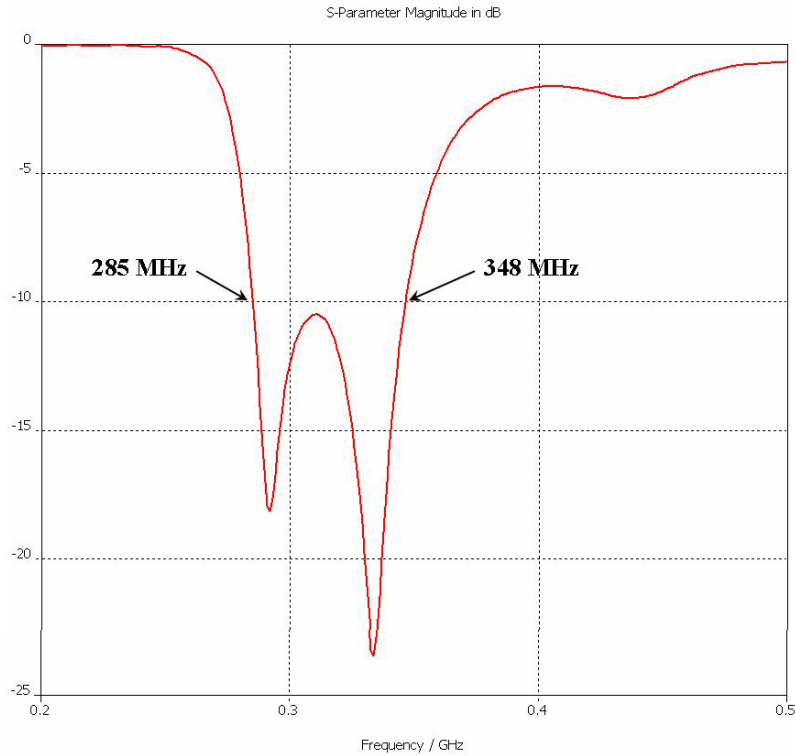
Figure 46   Return Loss for Optimized Design of 300 MHz U-Slot Microstrip Patch Antenna Indicating a Center Frequency of 346 MHz and Bandwidth of 63 MHz (20%).
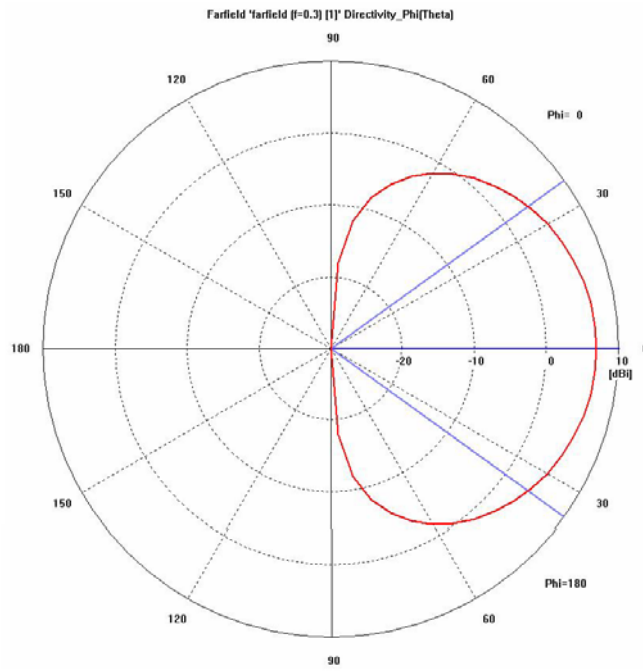

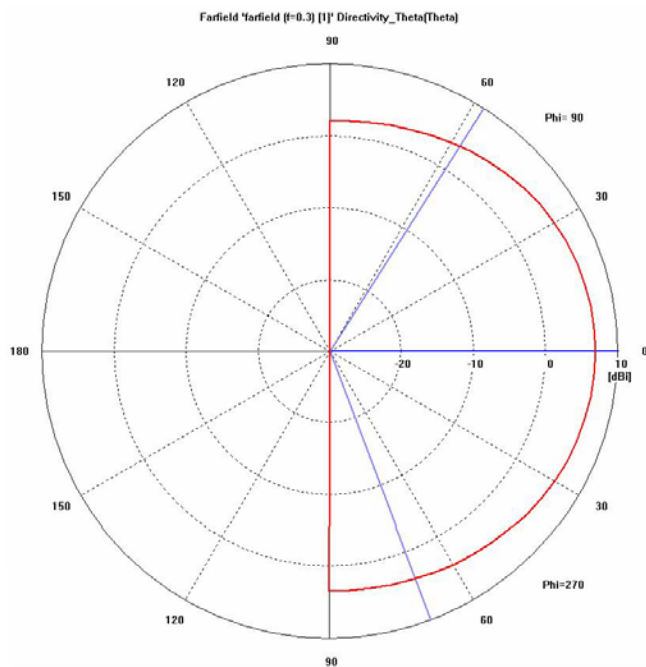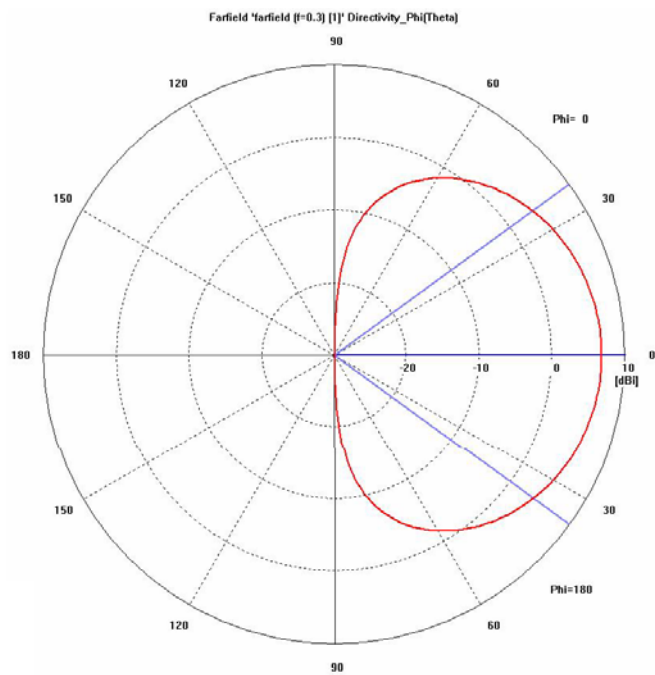Figure 47   Far-field Radiation Pattern of Optimized Design for $\phi = 0°$ at 300 MHz.

75
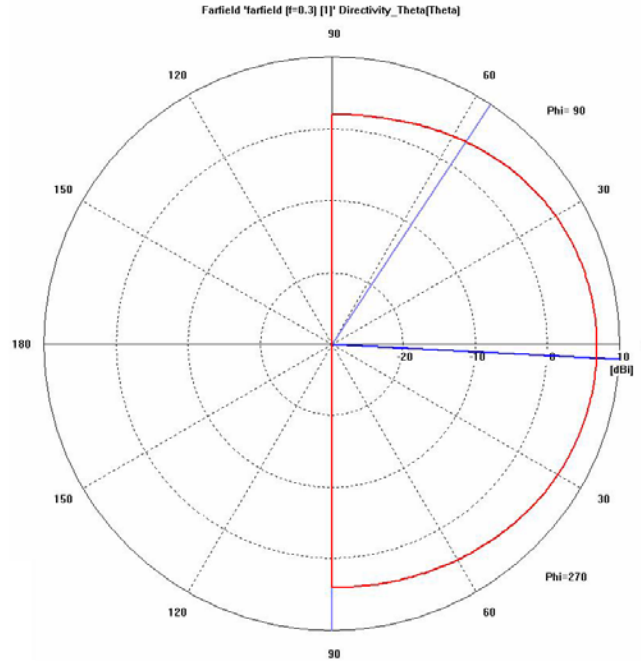
Figure 48   Far-field Radiation Pattern of Optimized Design for $\phi = 90°$ at 300 MHz.

I.   EVALUATION OF PROPOSED DESIGN PROCEDURES

The design procedures outlined in this thesis create a good initial design and provide a systematic method of fine-tuning the design to achieve broad-band operation. Nonetheless, it is important to understand the associated advantages and limitations.

1.   Advantages of Proposed Design Procedures

The advantages of the proposed design procedures include:

1.   Initial design procedures are based on theory, albeit theory established for the rectangular microstrip patch antenna.

2.   Initial designs typically achieve center frequencies that are close to the desired operating frequency.

3.   Optimization procedures are systematic and intuitive.

2.   Limitations of Proposed Design Procedures

The limitations of the proposed design procedures include:

1.   Physically unfeasible designs may be generated.

2.   Does not insure that broad-band operation can be achieved for any given initial design.

3.   Local optimum, instead of global optimum, may be achieved.

76

While the design procedures presented in this thesis are approximate and may not work in all situations, they do provide a good starting point for designing the U-slot patch antenna and give better and more timely results than simple guesses or arbitrary trial-and-error methods. Further study may be necessary to better understand the relationship between the U-slot geometry and the impedance characteristics of the patch antenna. Parameters such as the U-slot vertical arm length, C, and the U-slot base length, D, are likely to be important factors in achieving broad-band operation and further parametric studies on these parameters may be useful.

THIS PAGE INTENTIONALLY LEFT BLANK

VI. CONCLUSIONS AND RECOMMENDATIONS

A.   SUMMARY OF SYSTEM STUDY

The first objective of this thesis was to perform a system study of the aperstructure and opportunistic array concepts. A CAD model of a DD(X)-sized ship was built and various numbers of antenna elements were distributed randomly over the ship's structure.   The MATLAB programs "ArrayPatternSub.m" and "arraygainSub.m" were used to plot the beam pattern and determine the main lobe gain and average sidelobe levels numerically for various element configurations. The values for the main lobe gain were used in the MATLAB program "ArrayPerformance.m" to characterize the performance of the radar vis-à-vis the number of elements. The parameters for the AN/FPS-115 PAVE PAWS radar were used to develop a realistic radar performance model.

By combining statistical theory for thinned and random arrays with the results of the MATLAB simulations, it was determined that factors such as the number of active elements at specific scan angles, average sidelobe level and main lobe gain could be predicted accurately. Using these results, the radar performance vis-à-vis the number of antenna elements was characterized. The study also verified that a theoretical maximum detection range of 1000 km could be achieved with approximately 400 antenna elements. In addition, the study indicated that 360° operation is possible, albeit requiring trade-offs in angular resolution and range.

B.   RECOMMENDATIONS FOR ADVANCED SYSTEM SIMULATION AND TRADE-OFF STUDIES

1.   Frequency Band Trade-off

Two radar frequency bands that have been identified for the BMD application are the VHF (216 MHz to 225 MHz) and UHF (420 MHz to 440 MHz). Further study is necessary to determine the performance of either frequency bands with respect to factors such as the target RCS, atmospheric attenuation, ground and sea clutter, among others. Simulation tools such as the Advanced Refractive Effects Prediction System (AREPS) could be used to investigate the effects of atmospheric refraction.

2. Model Enhancement

Using the knowledge gained from the U-slot patch antenna design, further enhancements can now be made to the MATLAB model to accurately represent the radiation pattern and directive gain. This will enable a more realistic study of the endfire configuration. In addition, further modeling is necessary to characterize the effects of amplitude tapering on sidelobe reduction.

3. Signal Processing Study

Further study is required to investigate the use of signal processing techniques, such as pulse compression and pulse integration, to improve the radar performance. In particular, issues such as the limits of performance, signal processing bandwidth requirements and additional hardware requirements need to be studied.

C. SUMMARY FOR U-SLOT MICROSTRIP PATCH ANTENNA DESIGN

The second objective of this thesis was to design a low-profile, broad-band microstrip patch antenna. The simulation tool CST Microwave Studio was first validated against published experimental and computed data for the U-slot geometry. Next, the selection of substrate material and choice of coaxial feed were discussed. The relationships between the U-slot geometry and the impedance characteristics of the patch antenna were investigated using CST Microwave Studio. Thereafter, an initial design was created and optimized using the outlined procedures.

CST Microwave Studio was shown to achieve results similar to the published experimental and computed data, hence validating its accuracy for the U-slot topology. The substrate selected was a low permittivity ($\varepsilon_r = 2.33$) composite material substrate – woven web PTFE-glass – that provides excellent dimensional stability and chemical resistance while allowing operation in a wide temperature range. A semi-rigid coaxial cable that has high power handling efficiencies was chosen for the feed. The initial U-slot patch antenna design achieved a center frequency that was close to the desired operating frequency but had a bandwidth of only 7%. This design was optimized using a tuning technique that manipulates the location and size of the impedance locus on the Smith Chart. The optimized design achieved a bandwidth of approximately 20% while

maintaining a low-profile, compactness and a simple topology. A set of simple design procedures that result in a good "first-pass" design with prescribed characteristics was developed.

D. RECOMMENDATIONS FOR FUTURE DESIGN DEVELOPMENT

1. Antenna Patch Size Reduction

Reducing the patch size will reduce the area required on the ship's structure and reduce mutual coupling between individual antenna elements. Alternatively, the density of antenna elements on the structure could be increased, hence reducing the average sidelobe level. Further study is required to explore techniques of reducing the antenna patch size.

2. Use of New Generation Ceramic Substrates

The use of high permittivity substrates could lower the profile of the U-slot patch antenna even further. Dimensional stability requirements, however, could impose a lower limit on the thickness of the patch. Further study, both from electrical and mechanical perspectives, is necessary to investigate the feasibility of using new generation ceramic substrates to lower the profile of the patch antenna. Low-loss dielectric ceramic, with dielectric constants ranging from 6 to 270, have been reported by Pacific Ceramics, Inc.

3. Fabrication and Testing

Fabrication and testing is the logical step after designing the U-slot patch antenna. It is imperative to measure the radiation characteristics of the individual U-slot patch antenna as well as investigate the integration of the U-slot patch antenna into the overall digital radar architecture. The overall project plan includes a demonstration of the aperstructure and opportunistic array concepts, possibly using Spanegal Hall at the Naval Postgraduate School as an aperstructure.

E. FUTURE RESEARCH IN THE APERSTRUCTURE AND OPPORTUNISTIC ARRAY CONCEPTS

In this thesis, the aperstructure and opportunistic array concepts were developed in a naval context, in particular, for a BMD application. The many inherent advantages

of aperstructures and opportunistic arrays, however, make them excellent candidates for a wide variety of applications. The opportunistic nature, stealth, multifunction capabilities and high survivability of these arrays can be exploited by the Army and Air Force to deploy radar networks within urban centers in crisis areas – quickly and covertly. Such hastily formed radar networks can then be used for communications and/or to detect and track targets such as missiles, aircraft or artillery rounds. The modularity and flexibility of these arrays also make them highly useful in disaster relief scenarios. In the event of disasters such as the tsunami in December 2004, opportunistic arrays can be used to set-up air traffic control and communication facilities quickly – hence facilitating the timely evacuation of victims and delivery of aid. The components of the opportunistic array could be operational spares from a similar system deployed elsewhere, eliminating the need to redeploy air traffic control and communication systems from other existing facilities. As a result, it is envisioned that future research in the aperstructures and opportunistic array concepts will diverge from the present naval application and encompass both military and commercial land-based applications.

LIST OF REFERENCES

[1]   Admiral Vern Clark, "Persistent Combat Power," speech delivered at the U.S. Naval Institute's 129th Annual Meeting and 13th Annapolis Seminar, Annapolis, Maryland, 3 April 2003.

[2]   Admiral M.G. Mullen, "CNO Guidance for 2006, Meeting the Challenge of a New Era," announced in NAVADMIN 272/05, 14 October 2005.

[3]   Federation of American Scientists, http://www.fas.org/spp/military/program/ nssrm/initiatives/cobragem.htm, November 2005.

[4]   Lance C. Esswein, "Genetic Algorithm Design and Testing of a Random Element 3-D 2.4 GHz Phased Array Transmit Antenna Constructed of Commercial RF Microchips," Master's Thesis, Naval Postgraduate School, Monterey, California, June 2003.

[5]   Eng, Cher Shin, "Digital Antenna Architectures Using Commercial Off The Shelf Hardware," Master's Thesis, Naval Postgraduate School, Monterey, California, December 2003.

[6]   Ong, Chin Siang, "Digital Phased Array Architectures for Radar and Communications Based on Off-The-Shelf Wireless Technologies," Master's Thesis, Naval Postgraduate School, Monterey, California, December 2004.

[7]   Warren L. Stutzman and Gary A. Thiele, *Antenna Theory and Design*, 2nd edition, Wiley, New York, 1998.

[8]   *IEEE Standard Definition of Terms for Antennas*, 1993.

[9]   Constantine A. Balanis, *Antenna Theory Analysis and Design*, 2nd edition, Wiley, New York, 1997.

[10]   Donald L. Walters, lecture notes for PH4274 Physics of Active Electromagnetic Sensor Systems, unpublished.

[11]   Bernard D. Steinberg, *Principles of Aperture and Array System Design*, Wiley, New York, 1976.

[12]   Merrill I. Skolnik, *Introduction to Radar Systems*, 3rd edition, McGraw Hill, New York, 2001.

[13]   David C. Jenn, lecture notes for Antennas and Propagation, unpublished.

[14]   R. Garg, P. Bhartia, I. Bahl, A. Ittipoboon, *Microstrip Antenna Design Handbook*, Artech House, Norwood, Massachusetts, 2001.

[15]   R. Q. Lee, K. F. Lee, J. Bobinchak, "Characteristics of a Two-Layer Electromagnetically Coupled Rectangular Patch Antenna," *Electronic Letters*, vol. 23, no. 20, 1987.

[16]   W. Chen, K. F. Lee, R. Q. Lee, "Spectral Domain Moment Method Analysis of Coplanar Microstrip Parasitic Subarrays," *Microwave and Optical Technology Letters*, vol. 6, no. 3, 1993.

[17]   T. Huynh, K. F. Lee, "Single-Layer Single Patch Wideband Microstrip Antenna," *Electronic Letters*, vol. 21, no. 16, August 1995.

[18]   S. Weigand, G. H. Huff, K. H. Pan, J. T. Bernhard, "Analysis and Design of Broad-band Single-Layer Rectangular U-slot Microstrip Patch Antennas," *IEEE Transactions on Antennas and Propagation*, vol. 51, no. 3, March 2003.

[19]   V. Natarajan, D. Chatterjee, "An Empirical Approach for Design of Wideband, Probe-fed, U-slot Microstrip Patch Antennas on Single-layer, Infinite, Grounded Substrates," *ACES Journal*, vol. 18, no. 3, November 2003.

[20]   V. Natarajan, D. Chatterjee, "Effect of Substrate Permittivity and Thickness on Performance of Single-Layer, Wideband, U-slot Antennas on Microwave Substrates," *Proceedings of the 20th Annual Review of Progress in Applied Computational Electromagnetics* at Syracuse, New York, April 2004.

[21]   V. Natarajan, "Some Design and Modeling Aspects of a Class of Wideband Microstrip Antennas Using Commercially Available CAD Softwares," M.S. Thesis, EE Department, University of Missouri, Columbia, Missouri, December 2002.

[22]   V. Natarajan, E. Chettiar, D. Chatterjee, "Performance of Two Empirical Techniques for Optimized Design of Wideband, U-Slot Antennas Using Commercial CAD Tools," *IEEE Antennas and Propagation* and *URSI/USNC Symposium Digest*, vol. 3, Monterey, California, June 2004.

[23]   V. Natarajan, D. Chatterjee, "Comparative Evaluation of Some Empirical Design Techniques for CAD Optimization of Wideband U-Slot Microstrip Antennas," *ACES Journal*, vol. 20, no. 1, March 2005.

[24]   R. C. Johnson, "*Antenna Engineering Handbook,*" 3rd edition, McGraw Hill, New York, 1993.

[25]   R. P. Owens, "Accurate Analytical Determination of Quasistatic Microstrip Line Parameters," *The Radio and Electronic Engineer*, vol. 46, no. 7, July 1976.

[26]   E. O. Hammerstad, "Equations for Microstrip Circuit Design," *Proc. Fifth Europ. Microwave Conf.*, September, 1975.

[27] Harwich Public Schools, http://www.harwich.edu/depts/hhssci/pavepaws.html, November 2005.

[28] K. F. Tong, K. M. Luk, K. F. Lee, R. Q. Lee, "A Broad-Band U-Slot Rectangular Patch Antenna on a Microwave Substrate," *IEEE Transactions on Antennas and Propagation*, vol. 48, no. 6, June, 2000.

[29] E. K. Miller, "Characterization, Comparison and Validation of Electromagnetics Modeling Software," *ACES Journal*, vol. 3, no. 2, 1989.

[30] Computer Simulation Technology, "*CST Microwave Studio Version 5 Getting Started*," Darmstadt, Germany, November, 2003.

[31] Micro-Coax, "Specifications for UT-141-HA-M17 Semi-Rigid Coaxial Cable," Pottstown, Pennsylvania, 2005.

THIS PAGE INTENTIONALLY LEFT BLANK

INITIAL DISTRIBUTION LIST

1.   Defense Technical Information Center
         Ft. Belvoir, Virginia

2.   Dudley Knox Library
         Naval Postgraduate School
         Monterey, California

3.   Professor David C. Jenn
         Department of Electrical and Computer Engineering
         Naval Postgraduate School
         Monterey, California

4.   Professor Donald L. Walters
         Physics Department
         Naval Postgraduate School
         Monterey, California

5.   Professor Andres Larraza
         Physics Department
         Naval Postgraduate School
         Monterey, California

6.   Chairman, Physics Department
         Naval Postgraduate School
         Monterey, California

7.   James King
         Office of Naval Research
         Arlington, Virginia

8.   Professor Michael Melich
         Wayne E. Meyer Institute of System Engineering
         Naval Postgraduate School
         Monterey, California

9.   Professor Rodney Johnson
         Wayne E. Meyer Institute of System Engineering
         Naval Postgraduate School
         Monterey, California

10.   Yeo Siew Yam
         DSO National Laboratories
         Singapore

11. Professor Yeo Tat Soon
     Director of Temasek Defence System Institute
     National University of Singapore
     Singapore

12. Leo Tin Boon
     Temasek Defence System Institute
     National University of Singapore
     Singapore

13. LCDR Gert Burgstaller
     Code: EC596
     Naval Postgraduate School
     Monterey, California

14. MAJ Loke Yong
     Naval Postgraduate School
     Monterey, California

15. CPT Tong Chin Hong Matthew
     Headquarters Singapore Artillery
     Singapore Armed Forces
     Singapore